

---

# Characterization and Optical Properties of Layered InSe and GaSe Crystals Intercalated with Hydrogen and Hydrogen-Containing Molecules

---

Yuriy Zhirko, Vasiliy Grekhov, Nikolay Skubenko,  
Zakhar Kovalyuk and Taras Feshak

Additional information is available at the end of the chapter

<http://dx.doi.org/10.5772/61051>

---

## Abstract

Described in this review are our electron-microscopic, energy dispersion, and optical (IR absorption and low-temperature (4.5 K) photoluminescence) investigations of layered InSe and GaSe crystals intercalated using the considered below methods with various concentrations of hydrogen or hydrogen-containing molecules (HCM) of water, toluene, and alcohol. It has been shown that these crystals are efficiently intercalated–deintercalated (IC–DIC) not only with hydrogen but also with HCM. It has been ascertained that the layered crystals kept for a long term in natural conditions contain molecules of water and carbon dioxide gas in the subsurface area, where their concentration increases with time. It has been shown that the concentration of molecules intercalated into the crystal decreases when deepening inside its bulk both along crystal layers and the normal to them. Also adduced were empirical equations relating concentration distribution of molecules intercalated into the crystal with the duration of IC–DIC processes. Ascertained are the optimal dimensions allowing to efficiently perform IC–DIC of the whole crystal bulk. It has been shown that the IC–DIC process in time has the look of a hysteresis loop—fast initial growth of the HCM concentration with the following slowdown when intercalating and fast drop with the following retardation when deintercalating under permanent evacuation of the chamber with the crystal. The availability of two types of conductivity in n-InSe and p-GaSe crystals causes some features in the emission spectra of the crystals intercalated with hydrogen or HCM. In the case of n-InSe crystals, the availability of HCM results, in the whole, in predominant emission of free excitons, and in the opposite case of p-GaSe crystals, the recombination of carriers via deep centers becomes predominant.

**Keywords:** Layered crystals, intercalation, SEM, EDX, photoluminescence

---

## 1. Introduction

Unique chemical bonds—strong ion-covalent hybrids- $p^3$ -bonds inside crystalline layers and weak van der Waals ones between layers, which take place in layered InSe and GaSe single crystals, provide the possibility to introduce foreign atoms and molecules into their interlayer space by using intercalation. From the practical viewpoint, these crystals and their intercalates are promising materials for solid-state hydrogen accumulators, electric power, and solar cells as well as for numerous applications in other tasks.

As it was shown in [1], the electrochemical intercalation of hydrogen into InSe and GaSe crystals results in changing their physical properties. In particular, spectra of exciton absorption in these crystals demonstrate two-dimensional localization of exciton movement inside the plane of crystal layers, and NMR spectra show resonance absorption of electromagnetic radiation by hydrogen molecules available both in the interlayer and intralayer spaces of the crystals. In this case, the chemical shift of the energy level inherent to molecular hydrogen in these crystals depends both on the hydrogen concentration and crystal temperature, while the intensity of resonance absorption bands for this hydrogen depends on direction and value chosen for applied magnetic field relatively to the plane of crystal layers. Calculations performed using the model of 2D and 3D localization of hydrogen molecules in the layered crystals showed [1] that the processes of intercalation and deintercalation of molecular hydrogen take place with participation of full-symmetric optical vibrations in the crystal lattice, which modulate the width of potential wells and barriers. Results of investigations [1] also showed that the hydrogen concentration in these crystals reaches considerable values comparable with the concentration of molecules in the very matrix and in powders of the crystals the amount of hydrogen molecules after the sufficient duration of intercalation can exceed the amount of matrix molecules by 2–2.5 times.

The aim of this work was to study changes of physicochemical properties arising in InSe and GaSe crystals in the course of intercalation with hydrogen, water, and more complex hydrogen-containing molecules of alcohol and toluene, as well as to obtain information about spatial distribution of the concentrations inherent to intercalated molecules in these crystals and dynamics of their deintercalation from the crystals by using the methods of optical and electron microscopy, energy dispersion, VIS, and IR spectrometry. In Section 2, we have adduced some (necessary to discuss the results obtained in this work) information about InSe and GaSe crystals, their physicochemical properties, and ways for the intercalation of simple nonorganic and organic molecules into these layered crystals. Section 3 describes results of our optical-microscopic, electron-microscopic, and energy dispersion investigations of InSe and GaSe crystals intercalated with hydrogen-containing molecules of water, alcohol, and toluene.

Adduced in Section 4 are the results of investigations concerning GaSe crystals kept for more than 30 years in natural conditions of ambient medium (“aged” crystals). Concentrations and chemical composition of molecules embedded from ambient medium in the process of natural intercalation into the subsurface area of the aged crystals are estimated there. Also, the estimates of spatial distribution inherent to simple nonorganic molecules in the bulk of the

layered crystals within the volume scales of  $> 1 \text{ cm}^3$  down to  $< 1 \cdot 10^{-10} \text{ cm}^3$  are made in both 2D and 3D versions. Besides, the results of investigations aimed at infrared light absorption by the aged GaSe crystals within the range of valence vibrations intrinsic for molecules of water and carbon dioxide are discussed; adduced are the analytical expressions relating the dependences of water molecules concentration in these crystals with the duration of their intercalation–deintercalation; given are recommendations concerning the spatial dimensions of the crystals from the viewpoint of their efficient application in hydrogen energetics.

Section 5 of the work describes the results of low-temperature investigations aimed at photoluminescence spectra of InSe and GaSe crystals intercalated with hydrogen molecules as well as molecules of water, alcohol, and toluene (containing OH and CH groups) with the purpose to ascertain the influence of their intercalation (including their passivation) on optical properties of these crystals within the range of the fundamental electron (exciton) transition. In summary, using the examples of InSe and GaSe crystals, we have presented generalized conclusions about the character of processes related with the intercalation–deintercalation of simple nonorganic and organic molecules into the layered crystals as well as their influence on physicochemical properties of these crystals in the context of applying these layered matrixes (not containing carbon) in hydrogen energetics.

## 2. Experimental methods

InSe and GaSe layered crystals considered in this chapter belong to binary compositions A<sub>3</sub>B<sub>6</sub>, in which crystalline layers are composed of four monolayers of Se and In(Ga) atoms, located one above another, in the sequence Se-In(Ga)-In(Ga)-Se and united together by ion-covalent hybrid  $sp^3$ -bonds. Inside these crystalline layers, the orientation of atoms correspond to the spatial group  $D_{3h}$ . In this case, each In(Ga) atom inside the crystalline layer provides the three nearest Se atoms with two own valence electrons to fill their  $p$ -shells, while one remaining electron together with another excess electron of the adjacent In(Ga) atom forms the completed  $s$ -shell. As a result, orbitals of valence electrons are localized inside the layer and practically do not overlap with orbitals of valence electrons from neighboring layers. As a consequence, there is a weak molecular van der Waals bond between these crystalline layers. This clearly pronounced anisotropy of chemical bonds between crystalline layers as well as inside these layers allows the intercalation of layered crystals, i.e., introduction of foreign atoms or molecules into interlayer space of a grown crystal. For instance, in the case of InSe and GaSe crystals, the volume of van der Waals space (the so-called “van der Waals gap”) is equal to 40–45% of the total crystal volume, and the internal surface of this space is close to  $(2\text{--}2.5) \cdot 10^3 \text{ m}^2$  in  $1 \text{ cm}^3$ .

It is well known [1–4] that InSe and GaSe single crystals grown by the Bridgman method have four polytypes ( $\beta$ ,  $\delta$ ,  $\epsilon$ , and  $\gamma$ ) that differ between each other by the sequence of packing the crystalline layers. As a rule, InSe single crystals have the  $\gamma$ -polytype with rhombohedral (trigonal) crystalline structure (spatial group  $C_{3v}^5$ , the primitive unit cell of which contains one

$\text{In}_2\text{Se}_2$  that comprises three layers). The nonprimitive hexagonal unit cell comprises three crystalline layers and consists of three molecules  $\text{In}_2\text{Se}_2$ . GaSe single crystals have  $\epsilon$ -polytype. They belong to the hexagonal crystalline structure (spatial group  $D_{3h}^1$ ), the unit cell of which consists of two  $\text{Ga}_2\text{Se}_2$  molecules located in the framework of two crystalline layers.

Parameters of the crystalline lattice inherent to  $\gamma$ -InSe and  $\epsilon$ -GaSe crystals are well investigated. In the case of  $\epsilon$ -GaSe, they are as follows: the lattice parameter along the direction perpendicular to the layers is  $C_0 = 15.95 \text{ \AA}$ , and inside the layer plane it is  $a_0 = 3.755 \text{ \AA}$  [5]. For  $\gamma$ -InSe, they are, respectively,  $C_0 = 25.32 \text{ \AA}$  and  $a_0 = 4.001 \text{ \AA}$ . The distances between the nearest atoms inside the layer are as follows:  $C_{\text{In-In}} = 2.79 \text{ \AA}$  and  $C_{\text{In-Se}} = 2.65 \text{ \AA}$ , angle  $\langle \varphi \rangle = 119.3^\circ$ , layer thickness  $C_1 = 5.36 \text{ \AA}$ , distance between layers  $C_2 = 3.08 \text{ \AA}$ , and the distance between the nearest Se atoms in adjacent layers  $C_{\text{Se-Se}} = 3.80 \text{ \AA}$  [6].

Undoubtedly, the unique properties of this class of semiconductor compounds, in particular, InSe and GaSe crystals, attract special attention of researchers because the heterostructures based on them not only possess high photosensitivity and can be applied in solar cells [7–9] and accumulators of electric energy [10] but are also rather promising for the creation of  $\gamma$ -radiation sensors, as it follows from [11]. At the same time, as it was shown in recent studies [1, 12–14] that the layered InSe and GaSe crystals can be applied in hydrogen energetics as operating elements in solid hydrogen accumulators. The hydrogen concentration in powders of these crystals can reach values close to  $x = 5\text{--}6$ , where  $x$  is the amount of embedded hydrogen atoms per one formula unit in the matrix of intercalated crystal.

Figure 1 shows volume images of molecules related to hydrogen, water, alcohol, toluene, or carbon oxide gas that were embedded into InSe and GaSe crystals by intercalation. The following methods were used in these cases: electrochemical intercalation, intercalation under pressure when working with hydrogen, or natural immersion deepening the samples to solutions of water, alcohol, and toluene, or long-term (for 30 years) keeping the samples in ambient atmosphere.

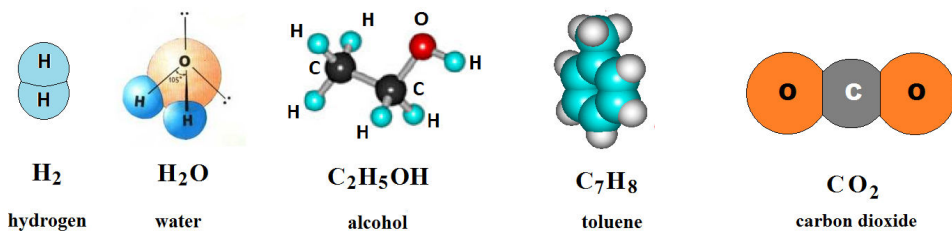


**Figure 1.** Volume images of molecules, namely, hydrogen, water, alcohol, toluene, and carbon oxide gas.

As seen from Figure 1, in their composition, majority of molecules have hydrogen. At the same time, the molecules of water and alcohol contain the hydroxyl group O-H, the molecules of alcohol and toluene—carboxyl group C-H, and the molecule of carbon oxide  $-\text{C}=\text{O}$  group.

## 2.1. The method of electrochemical intercalation

The method of electrochemical intercalation with using “pulling” electric field is presented in Figure 2. It was used when intercalating the crystals with hydrogen. Previous studies [12, 13] investigated layered InSe and GaSe crystals chemically intercalated with hydrogen, where the authors used the one-chamber three-electrode cell [1, 15] (see Figure 2a). When current passes through the cell, the composition of solution is changed due to redox processes taking place both on operation and on auxiliary electrodes. Products of reactions that go at the auxiliary electrode get to the zone of operation electrode and can interact with it, which results in changing its potential and can lead to incorrect determination of the embedded intercalant concentration.

Therefore, in this work, we used the cell separated by porous membrane spaces of operation and auxiliary electrodes (Figure 2b). The application of this cell enabled us to separate processes of oxidation and reduction and to prevent mixing solutions contacting with operation and auxiliary electrodes.

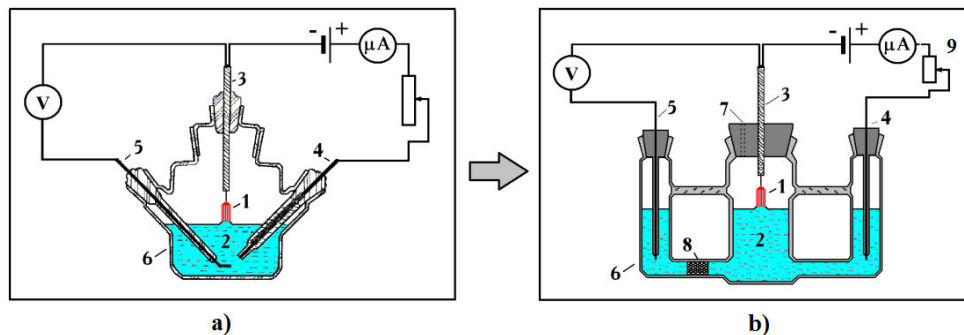


**Figure 2.** (a) One-chamber cell; (b) separated cell. The scheme of the electrochemical cell for the intercalation of layered InSe and GaSe crystals with hydrogen. 1—sample of InSe or GaSe (operation electrode, OE) 2—electrolyte; 3—operation electrode; 4—chlorine-silver reference electrode, CE; 5—auxiliary electrode (AE); 6—case of the cell; 7—hole for the sensor of pH-meter; 8—porous membrane; 9—potentiostat ПИИ-50-1.

It is noteworthy that the electrochemical cell used in the process of intercalating the layered crystals with hydrogen should satisfy the following requirements:

- Material of the cell should not interact with electrolyte. In our case, the cell was made of silica glass.
- Cell should be hermetic. It is acceptable to use Teflon, vinyl plastic, or chemical-resistant rubber.
- Space between operation and auxiliary electrodes should be separated with a porous membrane, for example, with the glass Schott filter.
- Cell design should provide measurements of the electrolyte pH level during the intercalation process.

When carrying out electrochemical intercalation, InSe and GaSe single crystals were used as the operation electrode. Their samples had the shape of parallelepiped. In accord with the method [16], thin copper wire was soldered to the sample from side opposite to that contacting with electrolyte. Another end of this wire was taken off through the cork and added to the potentiostat. As a reference electrode, we used the chlorine-silver electrode of industrial production. A thin platinum wire soldered in glass served as an auxiliary electrode.

To prepare electrolyte, we used concentrated hydrochloric acid of the “chemically pure” grade diluted in bidistilled water. H ions were embedded into the layered InSe and GaSe crystals as a result of cathode polarization in galvanostatic conditions ( $i_a = 50\text{--}100 \mu\text{A}/\text{cm}^2$ ) from 1 N HCl water solution under potentials of the operation electrode that did not allow release of gas-like hydrogen. The process was carried out like that used in electrolysis bath under permanent control of the operation electrode potential with using the chlorine-silver electrode deepened into 1 N HCl solution. In the course of intercalation, the electrolyte pH level was measured using the pH-meter HI-8314 through the special hole in the cell cork. The fact of intercalation with hydrogen ions was confirmed using chemical analysis.

The concentration of embedded hydrogen was determined via the amount of electrical charge passed through the cell, i.e., using the controlled parameters of intercalation process: the current density ( $j$ ) and the duration of the process ( $t$ ). This process is described by the following relation [17]:

$$C_0(i, t) = A \cdot e^{[\alpha(t) + \beta(t)]}, \quad (1)$$

where  $C_0(i, t)$  is the amount of embedded intercalating ions per unit volume of the crystal;  $\alpha(t)$ ,  $\beta(t)$  are some linear functions of embedding process duration;  $i$  is the current passing through the cell; and  $A$  is the coefficient of proportionality.

The influence of embedded protons concentration on properties of indium monoselenide was studied using the same group of samples by their step-by-step additional intercalation. This process was accompanied by a shift of the value of equilibrium electrode potential inherent to initial material. Taking into consideration the fact that the stationary potential  $E$  for the initial nonintercalated indium selenide is close to 0.25 V, and data of chemical analysis show that the higher hydrogen content is corresponded by the higher negative  $E$  value, one can draw a conclusion that the obtained shift of the equilibrium potential after intercalation is related with the creation of hydrogen compounds embedded.

## 2.2. Natural intercalation of InSe and GaSe single crystals

In this work, we also investigated intercalation processes in InSe and GaSe single crystals under pressure 2 to 5 atm in sealed silica ampoules filled with molecular hydrogen, or using the natural way by deepening the crystals into chemically pure solutions of water, alcohol, and toluene. In addition, we studied the samples of GaSe crystals that were kept for 30 years in

ambient atmosphere. To perform physicochemical investigations of naturally intercalated single crystals, from monocrystalline InSe and GaSe ingots, we cut discs and then prepared plates with the thickness 3 to 5 mm and lateral dimensions  $5 \times 5 \text{ mm}^2$ .

Natural intercalation with hydrogen under pressure was realized within the range of 2 to 5 atm in hermetic cells at the temperature  $200^\circ\text{C}$  for 3–4 hours. The natural immersion intercalation of the samples with molecules of water, alcohol, or toluene was performed at room temperature in silica ampoules by deepening them into chemically pure solutions of corresponding substances for 35 and 165 days. After finishing the process, the intercalated samples of InSe and GaSe were withdrawn from solutions.

### 2.3. The method for the deintercalation of hydrogen from layered crystals

Hydrogen deintercalation from electrochemically intercalated layered  $\text{H}_x\text{InSe}$  and  $\text{H}_x\text{GaSe}$  crystals were performed for 3–9 hours at  $T = 110^\circ\text{C}$  in vacuum under constant pumping out. It was ascertained that the degree of deintercalation in the  $\text{H}_x\text{InSe}$  samples practically linearly grows with the hydrogen concentration from 60% for  $x \rightarrow 0$  up to 75–80% for  $x \rightarrow 2$ . When increasing the hydrogen concentration up to  $x \rightarrow 4$ , the degree of deintercalation in  $\text{H}_x\text{InSe}$  and  $\text{H}_x\text{GaSe}$  crystals grows up to 85%. Investigation of powder-like InSe and GaSe crystals showed that the hydrogen concentration in them can reach the values  $x = 5\text{--}6$ , while the degree of deintercalation can reach 90%. Deintercalation of gases from the crystals kept for 30 years in natural conditions was carried out inside a vacuumed chamber. This method will be described below, when discussing the results of EDX investigations.

## 3. Physical properties of InSe and GaSe crystals intercalated with hydrogen and hydrogen-containing molecules

As it was shown by the previous electron-microscopic investigations of InSe and GaSe crystals electrochemically intercalated with hydrogen [1], even the 80,000-fold magnification, in the whole range of investigated hydrogen concentrations  $x$  from 0 up to 4, where  $x$  is the amount of molecules per one molecular unit of the matrix, electron images of crystalline surfaces have no formations of structural defects related with embedding hydrogen into these crystals. At the same time, small-angle XRD investigations showed [1, 14] that, with increasing the concentration of intercalated hydrogen, as a result of intercalated hydrogen pressure on the matrix, there grows deviation of matrix parameters in intercalate  $\text{H}_x\text{GaSe}$  from classical values in GaSe crystals (hexagonal group 9,6/mmm). In particular, for  $\text{H}_x\text{GaSe}$  crystals at  $T = 300 \text{ K}$  and  $x = 1.0$ , the parameter  $C_0$  is increased by  $0.031 \pm 0.003 \text{ \AA}$  from  $C_0 = 15.94 \text{ \AA}$  up to  $C_0 = 15.971 \text{ \AA}$ , and the parameter  $a_0$  by  $0.006 \pm 0.003 \text{ \AA}$  from  $a_0 = 3.753 \text{ \AA}$  up to  $a_0 = 3.759 \text{ \AA}$ .

It is noteworthy that, despite essential deviation of the lattice parameter after hydrogen intercalation from classical values, electron-microscopic images of crystal surfaces remain practically invariable even for high hydrogen concentrations, and any additional formations of nonuniformities on surfaces or inside the samples are not observed. At the same time, as it

was ascertained in [1], the samples of GaSe crystals contain residue of the monoclinic phase of red  $\beta$ -Se, and dimensions of these inclusions do not exceed 1  $\mu\text{m}$ . The inclusions disappear after annealing of the crystals in a silica ampoule for 3 hours in vacuum at the temperature  $T = 350^\circ\text{C}$ .

Investigation of EDX spectra taken from surfaces of InSe and GaSe crystals performed using the scanning microscope Zeiss EVO 50 XVP equipped with the detector INCA ENERGY 450 showed that chemical compositions of these crystals are as follows: 49.3% Se atoms and 50.7% In atoms in InSe crystals as well as 50.08% Se atoms and 49.92% Ga atoms in GaSe crystals.

### 3.1. Crystals intercalated with hydrogen-containing molecules

To study the influence of intercalation with hydrogen-containing molecules (HCM) of water, alcohol, and toluene on the crystals InSe and GaSe, we carried out optical, electron-microscopic (SEM), and energy-dispersed (EDX) investigations of the samples intercalated with HCM for 35 and 165 days. To reach it, we prepared six samples of InSe and the same amount of GaSe crystals intercalated naturally with molecules of above substances for 35 and 165 days, respectively, as well as reference samples of nonintercalated crystals and those electrochemically intercalated with hydrogen. When performing this part of work, we used electron microscopes of the firm TESCAN-SEM VEGA 3, SEM MIRA 3 with an immersion magnetic lens, two-beam SEM LIRA 3 equipped with energy-dispersed EDX spectrometers X-Max or BRUKER, as well as optical transmission microscope Primo Star 5 of the firm Carl Zeiss.

As can be seen in Figure 3, after the intercalation of the crystals with HCM (in particular, GaSe crystals with water for 165 days) even for 1,000-fold magnification in the optical microscope, one can observe the formation of a bubbled surface. More clearly pronounced such a surface can be seen in Figure 4 when using 50,000- or 100,000-fold magnification in the electron microscope SEM MIRA 3 with an immersion magnetic lens.

It is interesting that the same changes with the formation of bubbles after intercalation with water take place in InSe crystals, too. However, when intercalating the samples InSe and GaSe with alcohol or toluene, the formation of bubbled surfaces is essentially less pronounced as compared to the case of water.

It should be noted that under low magnification (Figures 5–7), sample surfaces with clear images of bubbles border with other surfaces where one can observe quite different formations (see light areas). For the case of 30,400-fold magnification, these areas are represented in Figure 6 as a color version. As can be seen, under this magnification, they take a look of some bushes or dendrites located at the crystal surface.

Demonstrated in Figure 7 as an example is the look of the surface for sample 2 (GaSe,  $\text{H}_2\text{O}$ , 35 days) obtained in the regime BSE + SE using SEM VEGA 3 with magnification 5,000. As one can see, after intercalation with water for 35 days, the sample surface is not so developed with dendrites as compared to that after long-term intercalation.

To ascertain the nature of these dendrites, we perform additional SEM and EDX investigations. Shown in Figure 8 are SE and BSE images of the GaSe crystal surface after intercalation with

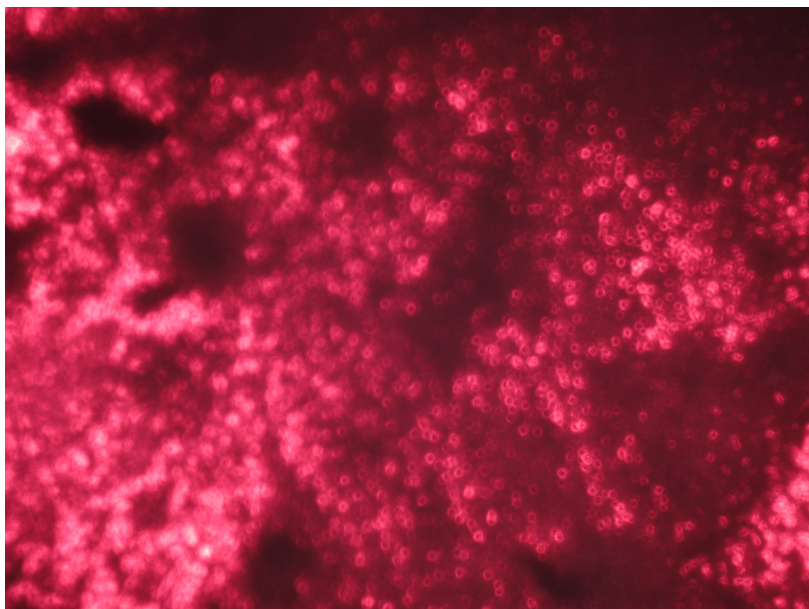


**Figure 3.** Optical transmission images of the GaSe crystal before (a) and after (b) its intercalation with water for 165 days, obtained using the transmission microscope Primo Star 5 at 1,000-fold magnification.

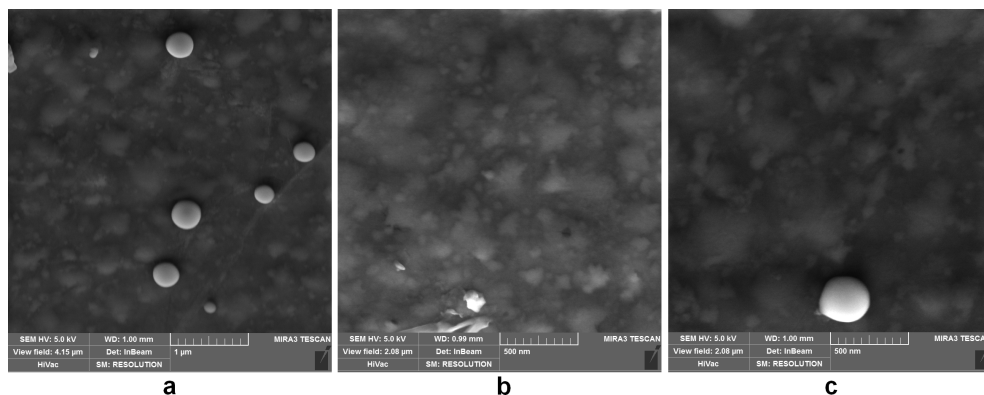


**Figure 4.** Obtained using SEM MIRA 3 images of several points on the sample surface for the crystal GaSe ( $\text{H}_2\text{O}$ , 165 days) with bubbles and remains of the  $\beta$ -Se phase for the accelerating voltage 5 kV: (a) point 1, magnification 50,000, scale—1 mkm; (b) point 2, magnification 100,000, scale—0.5 mkm; (c) point 3, magnification 100,000, scale—0.5 mkm.

water for 165 days. Seen there are the dendrites after processing them by using the two-beam electron microscope SEM LYRA 3. Lateral dimensions of the hollow etched out by the second beam are close to  $9 \times 14$  mkm, and its depth is 1.5 mkm. It is clearly seen that these dendrites grows through the surface from the crystal bulk, while their “roots” remain inside the crystal.

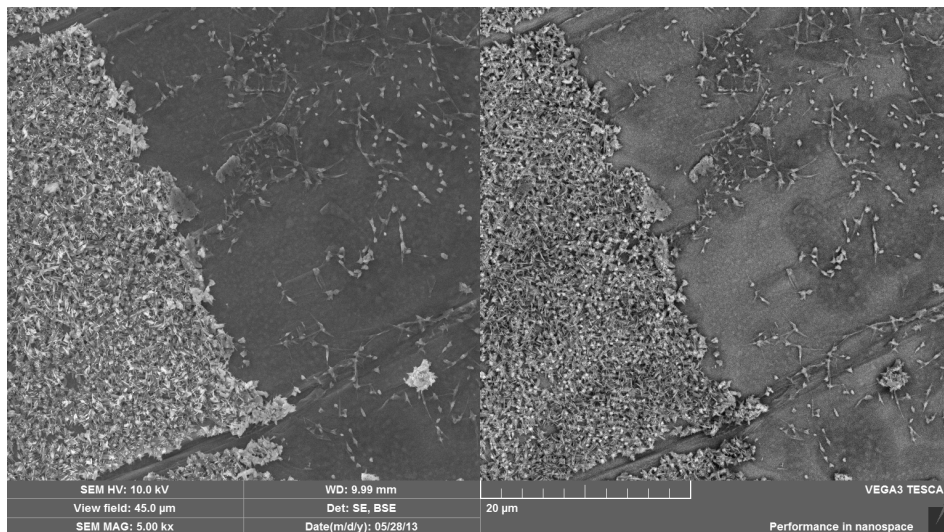


Figure 5. BSE + SE images for the surface of the sample GaSe (H<sub>2</sub>O, 165 days) obtained using SEM VEGA 3 with magnification 5,000 and accelerating voltage 10 kV. Scale—20 mkm.

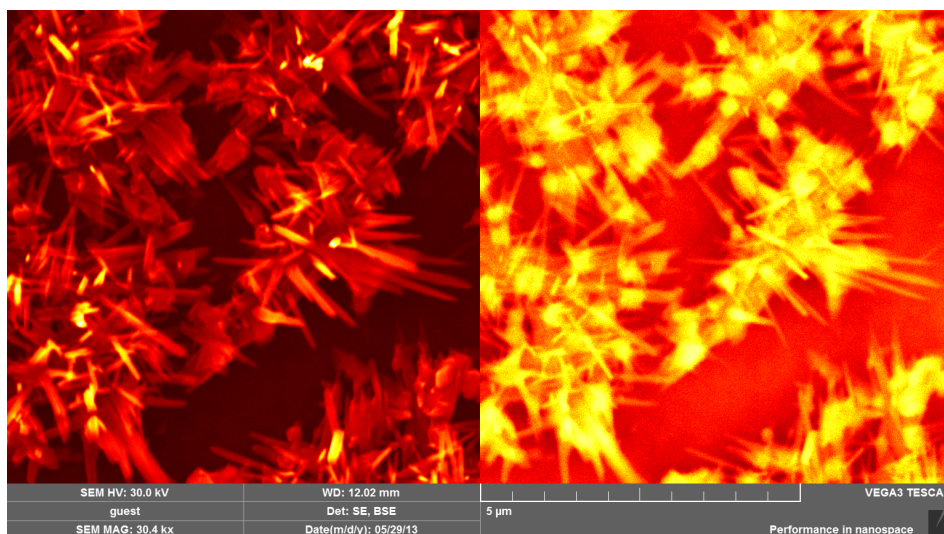
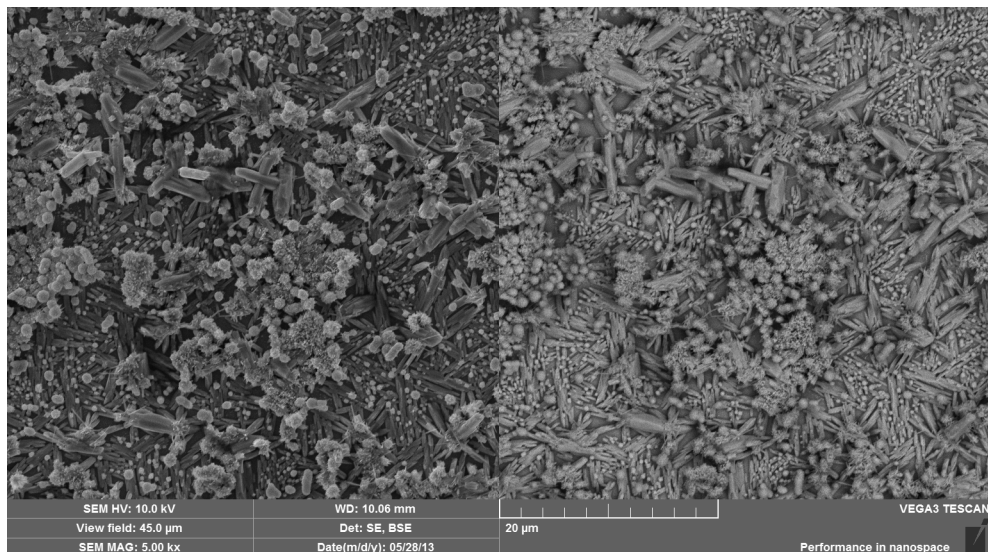
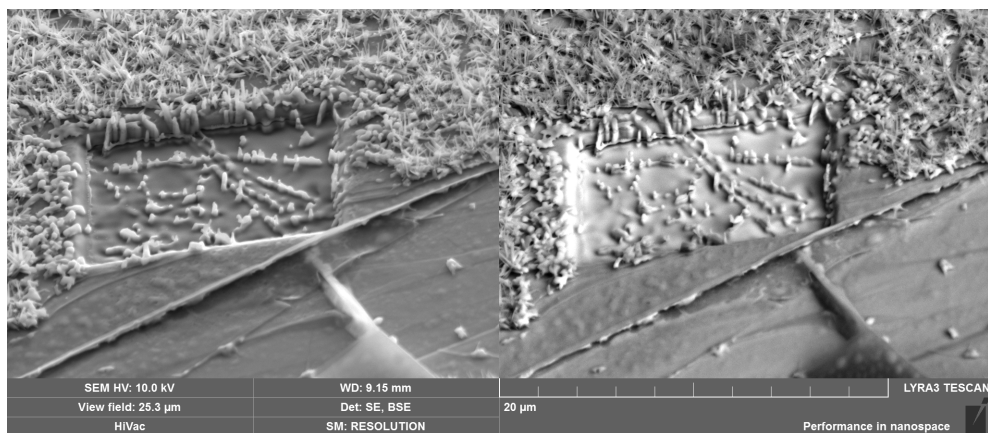


Figure 6. BSE + SE images for the surface of the sample GaSe (H<sub>2</sub>O, 165 days) obtained using SEM VEGA 3 with magnification 30,400 and accelerating voltage 30 kV. Scale—5 mkm. Color—after computer processing.



**Figure 7.** BSE + SE images for the surface of sample 2 (GaSe, H<sub>2</sub>O, 35 days) obtained using SEM VEGA 3 with magnification 5,000 and accelerating voltage 10 kV. Scale—20 μm.



**Figure 8.** SEM LYRA 3, magnification 5,000. Scale—20 μm.

To further ascertain the chemical nature of these dendrites, we use the same microscope SEM LYRA 3. It enables us to choose one of the dendrite samples that remained on the surface after cutting the hollow. Using the Ga-ion gun, this sample was fixed on the probe (see Figure 9). Then the end of the probe was attached to the sample holder, soldered to it by using the same gun and cut from the probe (Figure 10).

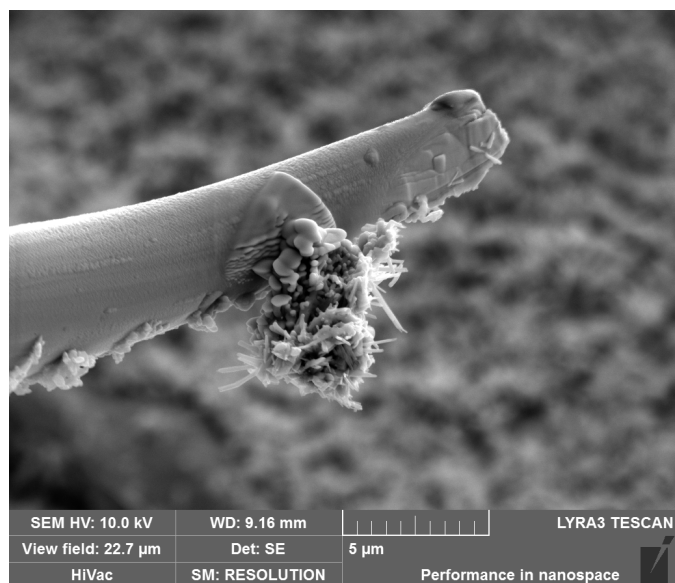


Figure 9. Spatial image of the dendrite fixed on the probe in SEM LYRA 3. Scale—1 mkm. Accelerating voltage 10 kV.

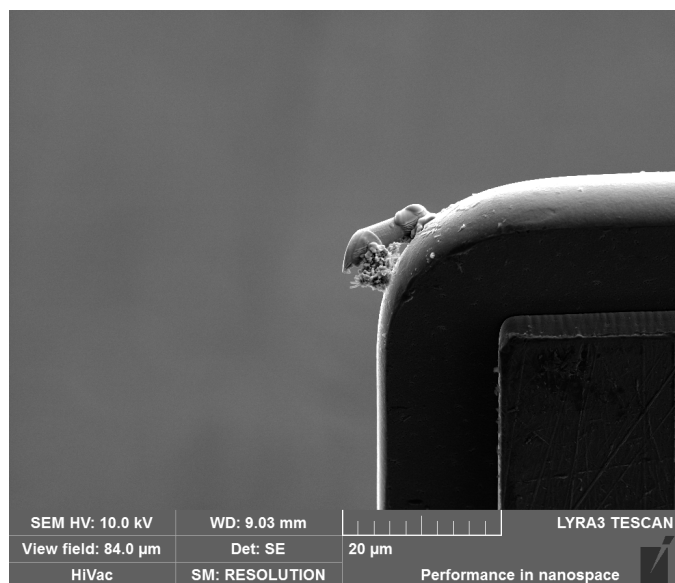
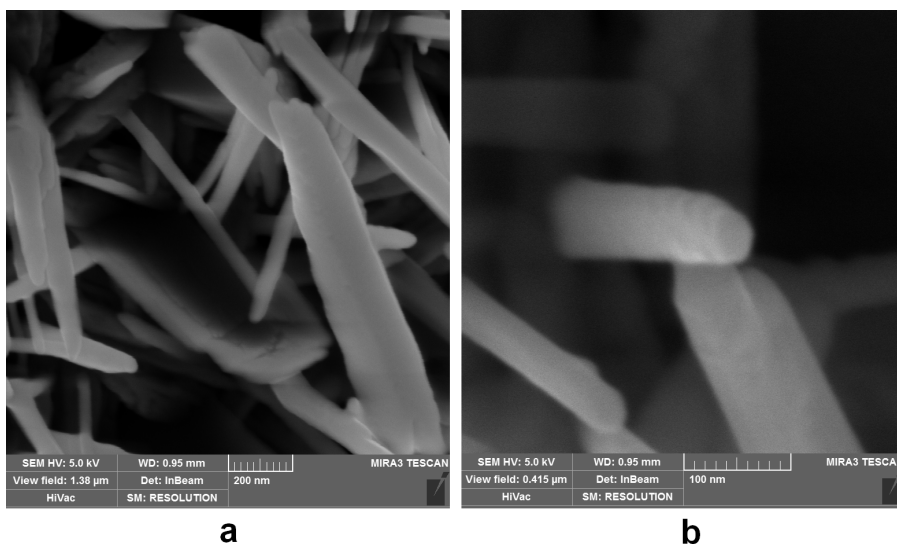


Figure 10. Spatial image of the residue of probe with the dendrite part fixed on the holder in SEM LYRA 3. Scale—20 mkm. Accelerating voltage 10 kV.

The dendrite sample on the probe, obtained in such a manner for EDX investigations, was transferred to SEM MIRA 3 equipped with the immersion magnetic lens. As seen in Figure 11a, for 150,000-fold magnification the dendrite structure is rather complex in 3D space. Under 500,000-fold magnification and the slope of the subject table 40° relatively to Z-axis, shown in Figure 11b is the image of one pin of the dendrite. It is clearly seen that the shape of the pin is close to cylindrical or cone-like. Its diameter at the end reaches 25–50 nm and is narrowed with the step 15 ± 2 nm. The same electron microscope SEM MIRA 3 enabled us to perform EDX investigations and ascertain that these dendrites mainly consist of Se atoms and, as seen from Figure 8, grow from the foreign phase of remaining β-Se.



**Figure 11.** SE images of surfaces in sample 1 (GaSe, H<sub>2</sub>O, 165 days) taken from areas with dendrites for very small WD. Microscope SEM MIRA 3, accelerating voltage 5 kV; magnifications: 150,000-fold (a) and 500,000-fold (b), scales—200 and 100 nm, respectively.

Energy dispersion investigations of GaSe crystal surfaces after water intercalation for 165 days also enabled to ascertain (see Tables 1 and 2) that in areas of dendrite localization, the oxygen concentration is approximately 3 times higher than in areas of minor amount of dendrites. When water molecules are present on the surface of crystals (in particular, GaSe), it can indicate the formation of developed complexes with β-Se accompanied by Ga<sub>2</sub>O<sub>3</sub> crystallites. As it follows from the tables, the increase in the Se concentration in these areas also correlates with these conclusions.

It should be noted that the formation of dendrites at the presence of water is more clearly pronounced in GaSe crystals than in the InSe ones, which is caused by different types of conductivity in these crystals. In accord with [18], it is dominance of acceptors over donors in GaSe crystals that causes precipitation of residual β-Se phases as well as binding and layering

the crystalline layers during growth of these crystals. The results of performed investigations allow concluding that the formation of bubbled surfaces in the course of intercalation with HCM is caused by partial layering along the van der Waals gap and filling this space of the crystal with molecules of water, alcohol, or toluene. It is seen from the example of GaSe that lateral dimensions of bubbled formations are commensurate with inclusions of residual  $\beta$ -Se in nonintercalated crystals and lie within the range 0.1 to 1.0  $\mu\text{m}$ .

Element	Series	Unn. [wt. %]	C norm. [wt. %]	C Atom [at. %]	C Error (1 Sigma) [wt. %]
Dendrites					
Carbon	K-series	0.00	0.00	0.00	0.00
Oxygen	K-series	6.16	9.52	33.15	1.03
Gallium	K-series	20.63	31.86	25.46	0.63
Selenium	K-series	37.96	58.62	41.38	1.23
Total :		64.75	100.00	100.00	
Bubbles					
Carbon	K-series	0.00	0.00	0.00	0.00
Oxygen	K-series	2.22	2.80	11.85	0.47
Gallium	K-series	33.94	42.77	41.51	0.98
Selenium	K-series	43.19	54.43	46.64	1.38
Total :		79.35	100.00	100.00	

**Table 1.** Distribution of chemical elements over the areas with dendrites and bubbles in sample 1

IC duration	HCM concentration		
	H <sub>2</sub> O	C <sub>2</sub> H <sub>5</sub> OH	C <sub>7</sub> H <sub>6</sub>
35 days		12%	6.0%
165 days		25%	12,5%
			5.2%
			9,9%

**Table 2.** HCM concentration in GaSe and InSe intercalates

Similar energy dispersion investigations were carried out using the crystals InSe and GaSe intercalated with toluene and alcohol for 35 and 165 days. The obtained concentrations of oxygen atoms after intercalation with water, of oxygen and carbon atoms after intercalation with alcohol, and of carbon after using toluene enabled us to estimate concentrations of HCM molecules as well as their dependences on the time of intercalation. The results of calculations shown in Table 2 confirm that the HCM concentration in the layered InSe and GaSe crystals grows by two times, when the duration of intercalation is increased from 35 to 165 days. It

allows making the first estimate of the dependence of the HCM concentration in these crystals on the time of deepening the sample in the respective solutions of HCM by using the following simple analytical expression

$$A(t) = A_0 \cdot \sqrt{A_0 \cdot t}, \quad (2)$$

where  $A(t)$  is the concentration of molecules intercalated into crystal,  $A_0$  is the fitting parameter for the crystal and solution, and  $t$  is the time of intercalation.

### 3.2. Conclusions

The performed optical, electron-microscopic, and energy-dispersed investigations enabled authors to ascertain that nonintercalated crystals do not possess stoichiometric composition. For instance, the chemical composition of crystals InSe and GaSe has the following atomic ratio: 49.3% Se atoms and 50.7% In atoms in InSe crystals as well as 50.08% Se atoms and 49.92% Ga atoms in GaSe. It is well correlated with their conductivity, namely, n-type for InSe and p-type for GaSe. The amount of residual  $\beta$ -Se in the interlayer space of GaSe crystals is much higher than that in the InSe ones.

It has been ascertained that the concentration of water, alcohol, and toluene molecules even in the case of the natural intercalation of InSe and GaSe crystals with time can reach considerable values ( $x \rightarrow 1$ ) commensurate with those after electrochemical intercalation.

It has been found that

- i. molecules containing hydroxyl group (OH) are embedded into InSe and GaSe crystals better than molecules containing the only carboxyl group (CH);
- ii. contrary to the case of hydrogen, high concentrations of HCM (when  $x \rightarrow 1$ ) lead to the blistering of the crystals and formation of bubbles in the interlayer space, which are filled with separate HCM or their liquids;
- iii. long-term intercalation with HCM (especially with water) results in the formation of dendrites on the surface of InSe and GaSe crystals, which have a look of bushes consisting of red monoclinic  $\beta$ -Se that forms (accumulates) in the process of synthesis of these crystals. Geometrical dimensions of these bushes can reach 2 to 5  $\mu\text{m}$ . Their pins have round or oval shape and diameter within the range 25–50 nm, they are narrowed to their ends with the step  $15 \pm 2$  nm;
- iv. since the amount of the residual  $\beta$ -Se in InSe crystals is lower than that in GaSe, the amount of formed dendrites in them is lower, too;
- v. in the areas where dendrites accumulate, one can observe an increased concentration of HCM.

### 3.3. Acknowledgement

The authors express their sincere gratitude to the firm TESCAN for the given possibility to carry out investigations by using the up-to-date samples of electron microscopes as well as to its co-workers Ph.D. Martin Petrevec, Michal Svoboda, Jiri Dlugos for their assistance in performing the part of this work, when studying the crystals InSe and GaSe intercalated with hydrogen-containing molecules.

## 4. Electron microscopy and energy dispersion investigations of GaSe crystals kept in natural ambient conditions

Presented in this chapter are the results of SEM and EDX investigations aimed at percentage and distribution of atmosphere gases in GaSe crystals kept for more than 30 years in natural ambient conditions of the medium geographic belt—in summer at temperatures up to +35°C, in winter down to -35°C, and air humidity from 30% up to 100%. With this aim, we chose to cut 30 years ago flat monocrystalline GaSe plates of the 12-mm width and 6-mm thickness, which were used for preparation of the samples with dimensions 10 × 12 mm and thickness 6 mm (in what follows, the crystals of the first type). Then the results of studying them were compared with those inherent to the GaSe crystals of the second type—as-grown crystals nonintercalated and intercalated with water. In detail, the crystals of the second type were described in the previous chapter.

### 4.1. SEM and EDX investigations

Energy dispersion (EDX) investigations of the atmosphere gases content in the crystals of the first type at surfaces containing planes of crystalline layers were performed using the scanning electron microscope SEM VEGA 3 (TESCAN). As these crystals are semiconductors, the investigations were performed without deposition of conducting layers on substrates, in the regime of medium vacuum, when the residual pressure in the column and chamber was close to  $2 \cdot 10^{-2}$  Pa. Registration of secondary electrons was made using the standard SE detector. Spectra of  $\gamma$ -radiation were measured using the energy-dispersed analyzer X-Max (OXFORD).

The optical image of the first type of GaSe crystal with the thickness 100 to 150 mkm obtained using the transmission optical microscope Primo Star 5 with 1,000-fold magnification is shown in Figure 12. It is seen that, in GaSe crystals of the first type as well as in those of the second type intercalated with water (see Figure 3 in Chapter 2), volume images contain nonhomogeneities that cannot be observed in as-grown crystals.

EDX investigations enabled to ascertain that the stoichiometric composition of Ga and Se atoms in the first type of crystals is the same as in as-grown crystals of the second type (studied in detail in [1]). At the same time, the results of these surface investigations showed the following:

1. There is a great amount of atomic oxygen in the crystals of the first type (see data in Figure 14d) as well as in the crystals of the second type intercalated with water.

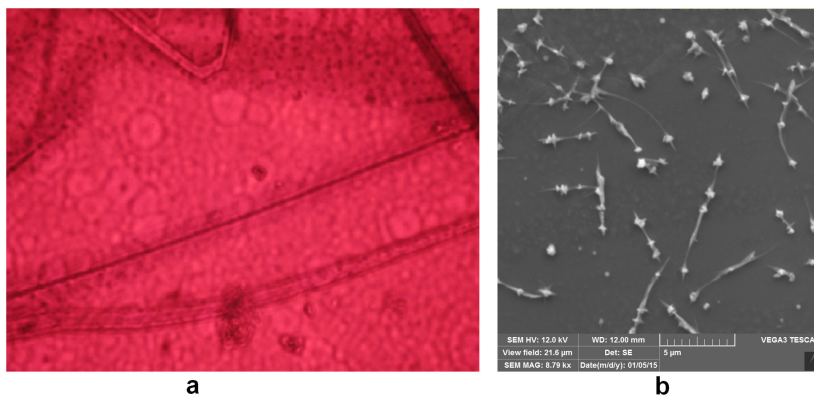


**Figure 12.** (a) Optical image of the first type of GaSe crystal obtained using the transmission optical microscope Primo Star 5 with 1,000-fold magnification. (b) SE image of the surface obtained for the same crystal under accelerating voltage 12 kV and magnification 8,790 times. Scale—5 mkm.

2. On surfaces of crystals of the first type (Figures 12b and 12a) as well as in the crystals of the second type intercalated with water (see Figures 4 and 5 in Chapter 2), one can observe nuclei of residual  $\beta$ -Se phase and dendrites of monocrystalline  $\beta$ -Se.
3. In the bulk of the first type of crystals (Figure. 13b, fresh cleavages at the depth close to 1 mm from the surface), contrary to the second type of as-grown crystals, these nucleation phases of residual  $\beta$ -Se cannot be already observed.

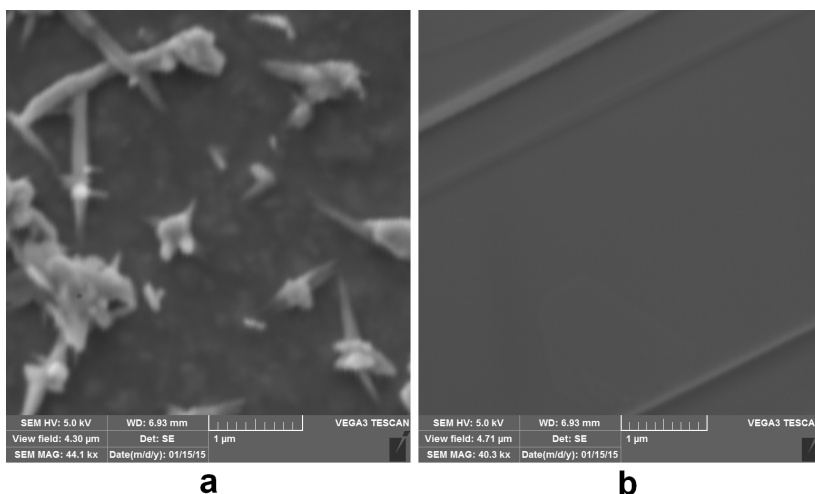


**Figure 13.** SE image for small WD taken: (a) from the crystal surface and (b) from the cleavage at the depth 1.1 mm, obtained at the accelerating voltage 5 kV and magnifications  $\times 44,100$  and  $\times 40,300$ , respectively. Scale—1 mkm.

Figure 14 shows the SE image of the first type of GaSe crystal under accelerating voltage 12 kV and magnification  $\times 2,000$ . Marked with the point in Figure 14a is the area used for EDX analysis. The spectrum of X-ray radiation corresponding to transitions of electrons between inner shells of atoms and analysis of chemical elements made in the virtual program shell INCA are represented in Figure 14c and in Figure 14d, respectively. It should be noted that the results adduced in Figures 13a and 13b were obtained in the first day of investigations.

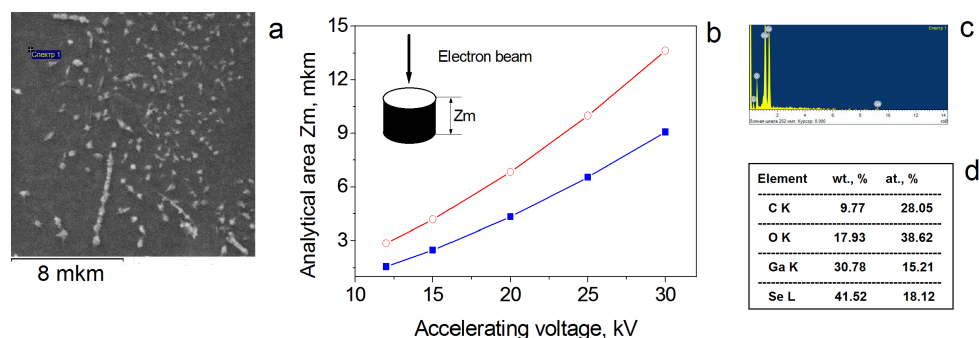
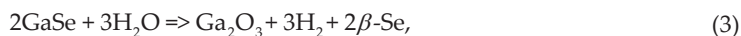


**Figure 14.** (a) Part of the first type of GaSe crystal and the point in it where EDX analysis was performed; (b) dependence of the size of analytical area  $Z_m$  (see the insert) on the accelerating voltage of the probing electron beam, which was obtained using Eq. (3.3) for oxygen (circles) and carbon (squares); (c) EDX spectrum of the point selected in Figure 14a; (d) chemical composition of elements in point 1 shown on a Figure 14a.

As it is seen from Figure 14d, in the points (and areas) containing no dendrites and residual phases of  $\beta$ -Se, surfaces of the first type of crystals contain a large amount of carbon and oxygen atoms. It is known that the Earth atmosphere mainly consists of molecules of nitrogen (78.1%), oxygen (21), argon (0.9%), water vapors (0.5–1.5%), and carbon dioxide (near 1%). Since, beside carbon and oxygen, other chemical elements present in the gas composition of the Earth's atmosphere were not found on the surface of the first type of GaSe crystals, it allows assuming that natural subsurface areas of these crystals as well as corresponding areas of the second type of crystals intercalated with water can contain a large amount of water molecules and carbon dioxide from ambient atmosphere.

Unfortunately, the data available in this chapter do not allow separating the intrinsic amount of carbon atoms in crystals of the first type from carbon available in the column and chamber of the microscope. At the same time, we can assume that the first type of crystal surfaces contain water and carbon dioxide molecules in approximately the same amounts. It permits us to exclude carbon from further discussion and to focus on the availability of oxygen. In this case, it is not excluded the possibility that subsurface area of the crystals in the presence of water molecules and molecular oxygen is subjected to substitution of Se atoms with the oxygen ones with the creation of a dielectric coating  $Ga_2O_3$  in accord with the scheme



or



Previous investigations of the second type of crystals are indicative of the fact that the process given by Eq. (3) is more preferable on the crystal surface in presence of water since it allows explaining the growth of dendrites from monocrystalline  $\beta$ -Se in the areas of nucleation phases of residual  $\beta$ -Se and probably decreasing amount of residual  $\beta$ -Se in the bulk of first type of crystals. The process given by Eq. (4) in our opinion was happened in a subsurface crystal area. Despite the described chemical processes of  $\text{Ga}_2\text{O}_3$  formation in the crystals of the first and second types, we assume that the main contribution to EDX spectra corresponding to presence of oxygen is conditioned by molecules of water and carbon dioxide embedded in the process of natural (atmospheric or immersion) intercalation into the layered crystal. In this case, as it follows from data on a Figure 14c, up to two atoms of oxygen are available per one molecule of  $\text{Ga}_2\text{Se}_2$  in the matrix of the first type of crystals.

Since GaSe crystals of the first type contain a large amount of oxygen atoms from the composition of  $\text{H}_2\text{O}$  and  $\text{CO}_2$  molecules, the authors performed temporal investigations of the processes related with the deintercalation of these molecules from the crystals. Every time after performing the EDX investigations, the first type of crystals remained in the pumped out chamber of microscope for 1 week. For this time, the residual pressure in the chamber increased from  $2 \times 10^{-2}$  up to  $2 \times 10^2$  Pa till the next day after measurements and up to  $3.5 \times 10^2$  Pa till the end of the week. Further, the next cycle of measurements was carried out.

Thus, seven cycles of measurements were repeated with the 1-week interval between them. The results of EDX investigations (by using the accelerating voltages for electrons from 15 to 30 kV) are adduced in Figure 15a, while their averaged voltage values are summarized in Table 3. Also, for comparison, presented in this table are the results of previous EDX investigations aimed at the second type of crystals after their intercalation with water for 35 and 165 days.

<b><math>K_0</math> - averaged concentrations of water molecules per one formular unit of GaSe crustal in subsurface regions</b>						
<b>1-st type</b>				<b>2-nd type</b>		
1 day	1 week	3 weeks	5 weeks	7 weeks	35 days	165 days
108 %	78 %	67 %	33 %	13 %	12 %	25 %

**Table 3.** The percentage of water determined using the EDX spectra of water intercalates of the layered  $\text{GaSe}[\text{H}_2\text{O}]_X$  crystals of the first and second types, where  $X$  is the amount of water molecules per one formula unit of the crystal

The performed EDX investigations of the first type of crystals under the values of accelerating voltages for electrons from 15 to 30 kV showed that, with increasing  $Z_m$ —depth of penetration typical for probing electron beam (calculated for oxygen atoms)—from 3.5 up to 13 mkm, the parameter  $K_0$ —concentration of oxygen atoms—decreases in the crystal. The increase in the

duration of evacuation also results in decreasing the oxygen concentration in the subsurface layer (see Table 3 and Figure 15b).

These results are shown in Figure 15a with open squares, rhombs, and circles for the cases of 7-, 21-, and 35-day keeping the first type of crystal in vacuum. The skew cross designates the water concentration in the subsurface area in the first day of investigations under the accelerating voltage 12 kV. It should be noted that the analytic area  $Z_m$  of the probing beam for chemical elements (in this case: gallium, selenium, oxygen, and carbon) was determined using the adopted fitting formula

$$Z_m = 0.033 \cdot (E_0^{1.7} - E_C^{1.7}) \cdot \frac{A}{\rho \cdot Z}, \quad (5)$$

where  $E_0$  is the accelerating voltage (kV),  $E_C$  is the minimum band emission energy (keV),  $A$  is the atomic mass,  $\rho$  is the density ( $\text{kg}/\text{m}^3$ ), and  $Z$  is the atomic number.

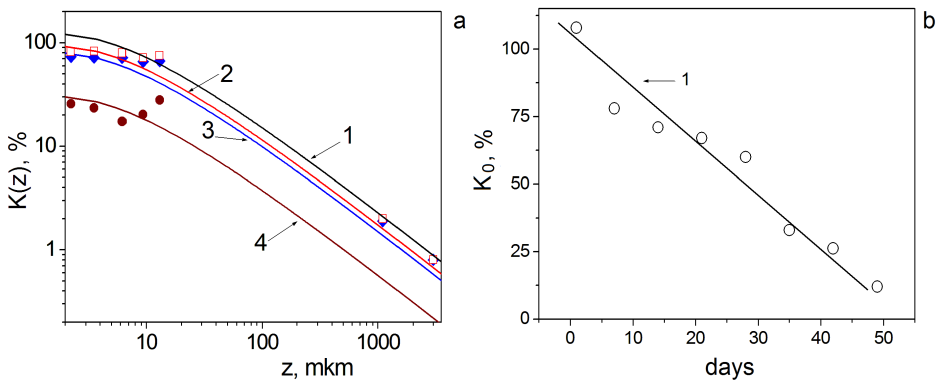


**Figure 15.** (a) Squares, rhombs, and circles correspond to experimental values of the water concentration in the subsurface area of the first type of crystal versus the depth of penetration typical for the probing electron beam in the case of 1-, 3-, and 5-week crystal being in vacuum, respectively. Crosses designate experimental values of the water concentration in the first day of measurements at the depth 2.24 mkm as well as on the fresh cleavage at the distance 1,100 mkm from the crystal surface and in the middle of the crystal at the depth 3,000 mkm obtained from IR investigations. The curves 1–4 correspond to fitting 2D dependences of the water concentration versus the crystal depth. The dependences were obtained in accord with Eq. (6) for the case of semi-infinite crystal. (b) The dependence of the fitting parameter  $K_0$  on the duration of keeping the first type of crystal in vacuum for the case of semi-infinite 2D crystal. Curve 1 is approximation of the parameter  $K_0$  dependence on time.

As seen from Figure 15a, with increasing the volume of the analytic area  $Z_m$ , the concentration of oxygen atoms in each of these measurements drops with increasing the depth of probing electron beam penetration into crystal. It allows ascertaining the relation between the parameter  $K_0$ —concentration of water on the surface of layered crystal and parameter  $K(z)$ —its distribution along the depth in the crystal bulk ( $z$ ) in the direction perpendicular to crystal layers in the following form

$$K(z) = \frac{e \cdot K_0 \cdot \ln(z+1)}{z+1}, \quad (6)$$

where  $e = 2.718...$  is the Napierian base. Note that this dependence is obtained for the case of semi-infinite crystal.

As seen from Figure 15a, the curves 1 to 3 both qualitatively and rather well quantitatively describe experimental values of the water vapor concentration  $K(z)$  in the crystal of the first type as a function of  $z$ -distance into the crystal bulk from its surface at fixed  $K_0$  values obtained after 1-, 3-, and 5-week being in vacuum. In Figure 15a, curve 1 plotted for the first day of measurements is indicative of a fast drop in the concentration of water molecules with depth. It is also seen (Figure 15a, curve 4) that, with increasing the duration of evacuation, the experimental values of the water vapor concentration  $K(z)$  in the crystal bulk begin to decline from the theoretical ones. It confirms that water and carbon dioxide molecules faster go out from subsurface areas and slower from the crystal bulk.

The similar phenomena of decreasing the water concentration are observed on the fresh cleavages of the first type of crystals (see Figure 13b) when shifting the point of measurements from an edge to the center. For instance, for the cleavage at the distance  $z = 1100$  mkm from the surface, the concentration of oxygen (measured immediately after obtaining the fresh cleavage) is decreased from 5.5% to 4% on the area  $500 \times 500$  mkm located in the center of the sample down to 1.5–1.1% on the area  $50 \times 50$  mkm in the same center. It indicates that in the first type of crystals, the concentration of intercalated water and carbon dioxide gas is also decreased in the lateral plane from the layer edge to its center. These results are shown in Figure 13a, with the asterisk for the case of the first day measurements on the area  $50 \times 50$  mkm at the value  $z = 1100$  mkm.

Thus, one can assume that the concentration of  $H_2O$  and  $CO_2$  molecules in the layered crystal decreases in the crystal bulk when moving from the surface into the bulk to its center—along the perpendicular and in the plane of crystal layers. Shown for clearness in Figure 16a is the 3D sketch of concentration distribution for  $H_2O$  and  $CO_2$  molecules in the layered crystal with increasing the depth—along the perpendicular ( $z$ -axis) and in the plane of layers ( $x, y$  axes).

We suppose that this simultaneous decrease in the concentration when shifting into the bulk as well as to the center of the sample is caused by the decrease in the amount of  $H_2O$  and  $CO_2$  molecules penetrating along the layers and perpendicularly to them at presence of covalent intralayer and van der Waals interlayer forces. Like to the case of molecular hydrogen intercalation in GaSe and InSe [1], this intercalation of  $H_2O$  and  $CO_2$  molecules takes place due to participation of  $A'_1$ -full-symmetric intralayer vibrations of  $Ga_2Se_2$  molecules.

These  $A'_1$  vibrations at room temperature are responsible for changing the width of potential barriers (interlayer Ga–Se bound) and the widths of 2D (van der Waals gaps) and 3D (interlayer space) quantum wells where the localization of molecules takes place. In the case of  $H_2O$  molecules, the localization of water vapors results in the formation of bubbles inside the

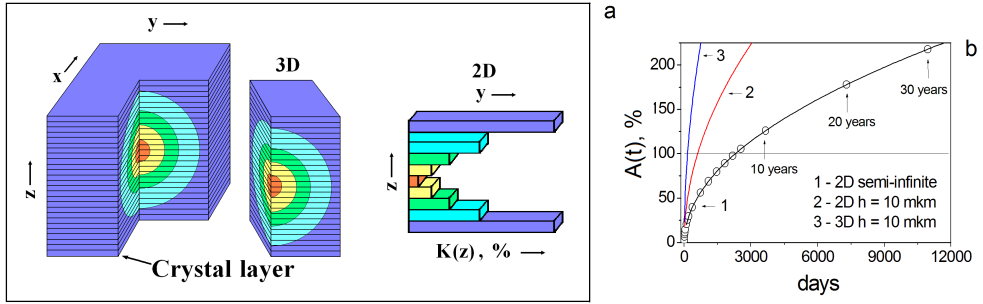


**Figure 16.** (a) The 3D sketch of distribution inherent to the concentration of water molecules in the layered crystal within the plane ( $x, y$ ) and along the perpendicular ( $z$ ) to crystal layers. Also shown here is the 2D crystal cut in the plane ( $y, z$ ). (b) Dependence of the water molecule concentration on the surface of the second type of crystal on the duration of the intercalation process. The circles and curve 1 correspond to the case of semi-infinite 2D distribution in accord with Eq. (2); curve 2—for the “thin” crystal with the thickness  $h = 10$  mkm; curve 3—for 3D crystal with the cube face  $h = 10$  mkm.

interlayer space, as it was shown in the previous chapter. The similar bubbles are also seen in subsurface areas of the first type GaSe crystals.

Thereof, being based on Eq. (5) describing the distribution of water molecules along the direction perpendicular to crystal layers (when the crystal is semi-infinite) and on the sketch for the generalized 3D distribution of the concentration inherent to  $H_2O$  and  $CO_2$  molecules inside the crystal GaSe, one can estimate the distribution of the concentration  $K(z)$  for these molecules in the case of a real crystal with the thickness  $z = h$ . Here, Eq. (5) should be transformed to the look

$$K(z)_{2D} = \frac{e \cdot K_0 \cdot \ln(z+1)}{(z+1)} + \frac{e \cdot K_0 \cdot \ln(h-z+1)}{(h-z+1)}, \quad (7)$$

which reflects the 2D cut of concentration distribution in a three-dimensional crystal. The integrated value of the molecular concentration for the 2D cut shown in Figure 16a at the fixed crystal thickness  $z = h$  can be defined as

$$K_{2D} = \int_0^h K(z) d(z). \quad (8)$$

Since in the first approximation one can assume that the distribution  $K(z)$  does not depend on direction within the plane ( $x, y$ ), the integrated value of specific molecule concentration in the bulk crystal of a cubic shape with faces  $h$  should have the following look

$$K_{3D} = (K_{2D})^{3/2}. \quad (9)$$

In accord with Eq. (8), Figure 17 shows the function for 2D distribution of concentrations for H<sub>2</sub>O and CO<sub>2</sub> molecules and various values of the crystal thickness  $h$ . For convenience, summarized in Table 4 are also the numeric values of the fitting parameter  $K_0$  on the surface as well as integrated values for the concentration of water molecules  $K_{2D}$  in the 2D cut and  $K_{3D}$  in 3D crystal bulk as a function of dimensions inherent to crystal faces ( $x, y, z$ ).

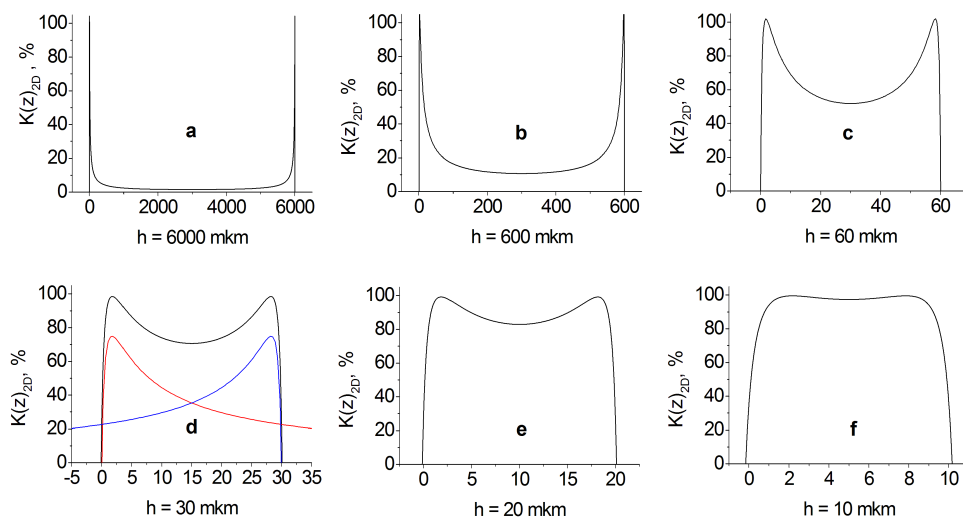


**Figure 17.** The 2D cut distribution of the concentration  $K_{2D}(z)$  in the case of infinite crystal with the thickness  $z = h$ .

As seen from Figures 17a to 17f, with decreasing the thickness of crystal, the integrated concentration of molecules  $K_{2D}$  in the 2D cut (area under the curve) increases from 3.4% for  $h = 6000$  mkm up to 94% for  $h = 10$  mkm. In this case, the integrated concentration in the bulk  $K_{3D}$  (see Table 4) also increases from 0.63% up to 91%. In addition, the contribution from opposite faces becomes more essential due to this decrease of geometrical dimensions of the crystal. In accord with Table 4, it results in a practically 2-fold decrease in the value of  $K_0$  parameter that defines the concentration of water molecules on the front face from  $K_0 = 100\%$  for  $h = 600$  mkm down to  $K_0 = 52\%$  for  $h = 10$  mkm. For clearness, this case is added in Figure 17d as superposition of distribution functions  $K_{2z}$  from the opposite crystal faces.

In summary of this discussion, we shall perform juxtaposition of results obtained after EDX investigations concerning deintercalation (in vacuum) of the first type samples with the similar data obtained in the process of immersion intercalation of these second type samples for the case of water molecules.

Length – (mkm): 2D case $x = y = \infty, z = h$ ; 3D case $x = y = z = h$	Adjusting concentration of $K_0$ on a surfaces for 2D case, (%)	Concentration $K_{2D}$ in case of 2D cross-section, %	Concentration $K_{3D}$ in 3D case, %
6000	100	3.4	0.63
600	99	18.5	38
60	90	67	55
30	80	80	72
20	70	88	83
15	66	92	88
10	60	94	91
5	52	91	87

**Table 4.** Values of the fitting parameter  $K_0$  and specific concentration  $K_{2D}$  on thickness ( $z = h$ ) for the 2D cut ( $x = y = \infty$ ), and for the specific concentration  $K_{3D}$  for a cube with face dimensions  $x = y = z = h$

#### 4.2. The model of the process for the intercalation–deintercalation of water molecules from GaSe crystals

In accord with the conclusions obtained in Section 3, the concentration of water intercalated into the crystal GaSe of the second type is described with the Eq. (2).

Let us consider that the parameters  $A_0$  and  $K_0$  describing processes of intercalation and deintercalation of water in GaSe crystals of the first and second types in the crystal subsurface area are compatible with each other. They unambiguously describe the process of intercalation–deintercalation of water in layered crystals. (Note that in the case of the second type of crystals, geometrical dimensions of crystals intercalated with water were  $5 \times 5 \times 1 \text{ mm}^3$ .) It follows thereof that in both cases of EDX investigations, the semi-infinite method of intercalation–deintercalation of surfaces took place. Therefore, contribution to the fitting parameters  $A_0$  and  $K_0$  from the opposite faces can be neglected. Then the processes of intercalation–deintercalation in the crystal semi-infinite by its thickness are identical to each other and can be described as follows

$$A(t, z) \equiv K(z, t). \quad (10)$$

where the functions  $A(t)$  and  $K(z)$  have now the look  $A(t, z) \equiv K(z, t) = f(z, t)$ . Then Eqs. (6) and (2) can be transformed to the look

$$K(z, t) = \frac{e \cdot K_0(t) \cdot \ln(z+1)}{z+1}, \quad \text{a}$$

and

$$A(t, z) = A_0(z) \cdot \sqrt{A_0(z)} \cdot t. \quad \text{b} \quad (11)$$

Thereof, if using the fitting parameter value  $A_0 = 1.63 \pm 0.5$  obtained to describe water intercalation into semi-infinite crystal of the second type, it follows that  $A(t)$  in the subsurface area

will reach the value equal to 100% in  $t = 6.5 \pm 0.5$  years. After keeping the sample in water for 30 years, in accord with Eq. (2) and curve 1 in Figure 14b,  $A(t)$  will reach the value  $215 \pm 5\%$ , which is 2-fold higher than after keeping the sample in ambient atmosphere.

Combining Eqs. (2), (8) and Eqs. (2), (9) with Eqs. (11a), (11b), one can prove that with decreasing the thickness of quasi-infinite crystal down to  $h = 10$  mkm (when the parameter value of  $K_0 = 50\%$  is sufficient), the function  $A(t, z)$  (curve 2 in Figure 14d) will reach 100% in  $600 \pm 20$  days, and when the crystal will be shortened to the cube with faces of 10 mkm, 100% intercalation will occur in  $150 \pm 5$  days (curve 3, Figure 14b).

Figure 18 shows a generalized process of intercalation–deintercalation of water in crystals GaSe for the 3D case, when  $x = y = z = h = 10$  mkm. Curve 1 is plotted in accord with Eq. (11b), and curve 2 is in accord with Eq. (11a). Experimental points correspond to the values shown in Figure 13b.

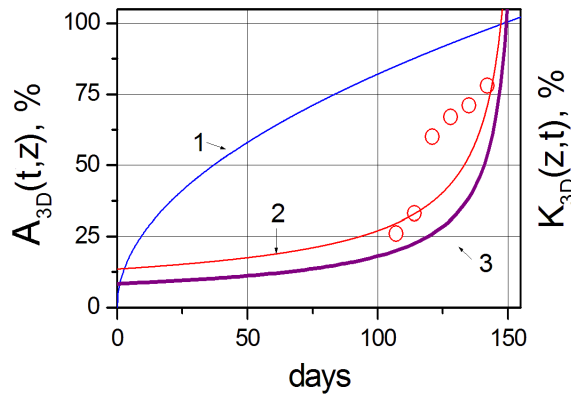


**Figure 18.** Scheme for the process of water intercalation–deintercalation into GaSe crystal. Curve 1 illustrates the process of intercalation in the cubic crystal with the face 10  $\mu\text{m}$ , and curves 2 and 3 describe the process of deintercalation from the infinite cubic crystal of the thickness 10  $\mu\text{m}$  and cubic crystal with the face 10  $\mu\text{m}$ , respectively. Open circles show experimental values  $K_0(t)$  on the surface of the crystal semi-infinite by its width.

As seen from Figure 18, the curve of intercalation–deintercalation looks like a hysteresis loop – a rather long process of natural intercalation with water is followed by rather fast deintercalation in vacuum under permanent pumping out. It is seen that the initial fast process of deintercalation at high concentrations is changed for the slow one at low concentrations. To provide full evacuation of water vapors, it needs period at least three times longer. It should be noted that curves 1 to 3 in Figure 18 only qualitatively describe these processes. In practice, these intercalation–deintercalation processes in crystals with small dimensions of faces are considered by us theoretically and need additional experimental investigations.

Since similar dependences of the water concentration on the duration of intercalation were also obtained for InSe crystals, we believe that the character of water intercalation–deintercalation processes in these crystals is analogous to that in GaSe crystals.

Additional investigations of light absorption by GaSe crystals of the first type were performed within the IR range of 2 to 5  $\mu\text{m}$ , where vibrations of water molecules in the condensed state and in the form of individual molecules as well as the carbon dioxide ones are active. Dimensions of the studied crystals were identical to those described earlier. The investigations did not find the bands related with water molecules in the condensed state. At the same time, after subtraction of contribution made by atmosphere water vapors and carbon dioxide gas, there remain weak bands related with molecules of  $\text{H}_2\text{O}$  and  $\text{CO}_2$  inside the crystals. Within the error of experiments ( $2\text{ cm}^{-1}$ ), using the  $\text{CO}_2$  molecules as an example, one can state that the intercalation of these molecules into the layered matrix results in neither changes in frequencies of “fan” vibrations inherent to these molecules nor the changes in the value of splitting between them.

### 4.3. Conclusions

The obtained results enabled us to make the following conclusions:

1. The layered crystals are well intercalated with water vapors from Earth atmosphere and deintercalated in the process of evacuation.
2. Water in the crystals of the first type is available in the molecular state close to that in Earth atmosphere.
3. Water molecules are in the state that is not bound with the very crystal.
4. Under long-term storage in ambient atmosphere, the concentration of water molecules in the subsurface area (10–20  $\mu\text{m}$ ) of layered crystals becomes comparable with the concentration of molecules in the very matrix.
5. In the crystals, volume of which is larger than  $(1 \times 1 \times 1)\text{ cm}^3$ , the integrated concentration of water molecules under a long-term storage can exceed the concentration of water vapors in atmosphere by 2 to 3 times.
6. The concentration of  $\text{H}_2\text{O}$  molecules sharply drops when deepening inside the crystal bulk.
7. Decreasing the crystal dimensions down to  $(10 \times 10 \times 10)\text{ }\mu\text{m}^3$  allows to enhance the rate of intercalation–deintercalation of water molecules in crystals of these dimensions.

## 5. Low-temperature investigations of photoluminescence spectra taken from InSe and GaSe crystals intercalated with hydrogen and hydrogen-containing molecules: comparative analysis

Photoluminescence spectra of InSe and GaSe crystals nondoped or doped with various impurities have been rather well studied by many authors for approximately 50 years. Therefore, being based on the previous results, one can study the influence of intercalation with hydrogen and hydrogen-containing molecules (HCM) on electron (exciton) excitations

in crystalline matrixes of these crystals. Electron transitions in HCM themselves or in their compositions from the ground state to the excited one as well as their following radiative recombination cannot give any contribution to spectra of crystal edge photoluminescence since their transition energies are much higher than the energy of fundamental transitions in these matrixes.

Low-temperature spectra of photoluminescence (PL) were measured at  $T = 4.5$  K by using 0.6-m MDP-23 monochromator with the diffraction grating  $1200 \text{ mm}^{-1}$ . PL excitation was provided with stabilized solid semiconductor lasers of the power 100 mW with the wavelengths 532 and 671 nm. To avoid registration of the second orders from the diffraction grating, we used the edge filters Semrock's LP03-532RS and LP02-830RS. To detect the useful signal, we used the photomultipliers  $\Phi\text{EY-79}$  and  $\Phi\text{EY-62}$  connected via analog–digital converter with PC. The stabilization of temperature was provided with the accuracy 0.1 K in a liquid helium cryostat by using the system YTPKEC designed at the Institute of Physics (NAS of Ukraine). The spectral slit width during experiments did not exceed 0.2 meV.

When carrying out this part of the work, we used the samples of InSe and GaSe crystals of the second type of nonintercalated and intercalated with hydrogen, water, alcohol, and toluene in various concentrations.

### 5.1. GaSe crystals

Shown in Figures 19a to 19f are the PL spectra of GaSe crystals intercalated with toluene, water, and alcohol for 35 and 165 days and measured at  $T = 4.5$  K. For comparison, PL spectra of nonintercalated GaSe crystal (Figure 19g) are shown, as well as the crystal doped with Cd (concentration 0.01 mass %) and irradiated with  $\gamma$ -quanta possessing the energies from the range 0 to 34 MeV and doses up to  $10_{14} \gamma\text{-quanta/cm}_2$  (Figure 19h). The latter crystal was earlier investigated in [11]. Added in the inserts of Fig. 4.1 (b, d, f) are also the 2D sketches of spatial-coordination ordering inherent to molecules of water, toluene, and alcohol. Figure 19 also illustrates spatial images of these molecules.

As it can be seen in Figure 19, at the temperature  $T = 4.5$  K PL spectra of GaSe crystals intercalated with toluene and water, like to the non-doped crystals or those doped with Cd, consist of emission lines related with free excitons (A-line,  $\lambda = 587.8$  nm), excitons localized near stacking faults of crystal layers ( $A_d$ -lines), and bound excitons (B1 – B6-lines). Besides, one can observe there wide doublet bands  $P0'$ ,  $P0''$  that, as shown in [11] using the example of GaSe: 0.01 % Cd crystals, are caused by radiative recombination of carriers from direct (DCB) and indirect (ICD) conduction bands to the acceptor level  $a1$  located at 70 meV above the top of valence band (VB). In accord with [11], this transition takes place with participation of TO phonons. The energy positions of peaks A,  $A_d$ , B1-B6 lines and doublet of the band P0 are summarized in Table 5.

As seen from Figure 19, the intercalation of GaSe crystals with toluene and water for 35 days, if comparing with nonintercalated crystals, results in noticeable changes of PL spectra within the range of free and bound excitons, namely, the intensity of A-line related with emission of

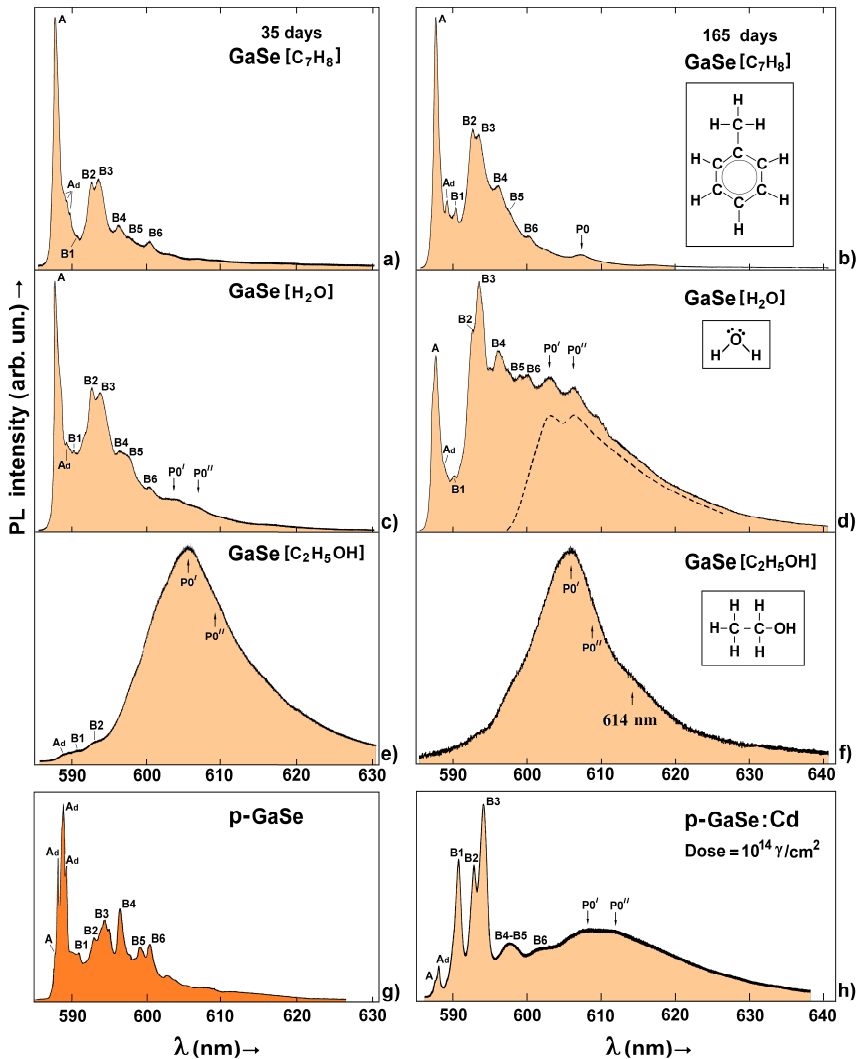


**Figure 19.** Measured at  $T = 4.5$  K PL spectra of the crystals: a, b—GaSe[C<sub>7</sub>H<sub>8</sub>]; c, d—GaSe[H<sub>2</sub>O]; e, f—GaSe[C<sub>2</sub>H<sub>5</sub>OH] intercalated for 35 and 165 days, respectively; g—GaSe; and h—GaSe:0.01Cd [11].

free exciton in the  $\epsilon$ -GaSe crystal grows, while the intensity of  $A_d$  lines related with emission of excitons localized within the ranges of stacking faults in crystal layersops.

It should be noted that the same phenomenon was observed in [11], when doping the crystals with impurities Cd and Zn available in the concentration 0.01 mass % as well as after their “radiation annealing” with  $\gamma$ -quanta of the energy from the range 0 to 34 MeV. In accord with [11], it is related with “curing” the defects by Schottky and by Frenkel, respectively. However,

the effect of increasing the intensity of A-line emission and the respective drop in intensity of A<sub>d</sub> lines is much better observed in the intercalates GaSe[H<sub>2</sub>O] and GaSe[C<sub>7</sub>H<sub>8</sub>] than in the case of doping with Cd and Zn and the following annealing of these GaSe crystals with γ-quanta.

Crystal	Wave length of emission line and band peaks (nm)								
	A	A <sub>d</sub>	B1	B2	B3	B4	B5	B6	P0', P0''
GaSe	587.8	588.1, 588.6, 589.3	590.9	592.6	594.1	596.5	599.1	600.4	
GaSe[C <sub>7</sub> H <sub>8</sub> ] – 35 days	587.8	588.0, 588.9, 589.7	590.5	592.6	593.7	596.4	597.6	600.5	
GaSe[C <sub>7</sub> H <sub>8</sub> ] – 165 days	587.9	589.2	590.4	592.5	593.5	596.1	597.5	600.2	607.2
GaSe[H <sub>2</sub> O] – 35 days	587.9	589.5	590.3	592.1	593.2	596.2	597.4	600.3	603.5, 606.9
GaSe[H <sub>2</sub> O] – 165 days	587.9		590.1	592.6	593.7	596.3	599.0	600.1	603.1, 606.3
GaSe[C <sub>2</sub> H <sub>5</sub> OH] – 35 days	588.9		590.7	593.0					605.8
GaSe[C <sub>2</sub> H <sub>5</sub> OH] – 165 days									606.0
GaSe:0.01Cd and dose = 10 <sup>14</sup> γ/cm <sup>2</sup> (data from [11])	587.6	588.5		591.5	593.6			600.4	608.0, 612.0

**Table 5.** Positions of emission peaks for free and bound excitons at T = 4.5 K typical for GaSe crystals non-intercalated and intercalated with HCM.

The following growth in the time of intercalation in these solutions for 165 days results in increasing the emission intensity within the range of P0-bands. Despite the fact that this effect is more clearly observed in the intercalates GaSe[H<sub>2</sub>O] (see the dashed line in Figure 19d) than in the intercalates GaSe[C<sub>7</sub>H<sub>8</sub>], the integrated intensity of the emission spectra corresponding to these intercalates (obtained for 165 days) remains the same as in those intercalated for 35 days.

At the same time, attention is attracted by the fact that the shape of PL spectrum typical for the crystal GaSe[H<sub>2</sub>O] intercalated for 35 days is practically identical to that of the crystal GaSe[C<sub>7</sub>H<sub>8</sub>] obtained by intercalation for 165 days. As follows from Table 2 (see Section 3.2), it correlates with measurements of concentrations of H<sub>2</sub>O molecules (12.0%) obtained by the intercalation of GaSe for 35 days and of C<sub>7</sub>H<sub>6</sub> molecules (9.9%) obtained by intercalation for

165 days. Also, we take into account that the redistribution of the emission intensity, which is observed in the long-wave range of the spectrum, is caused by transitions of carriers from DCB ( $P0'$ ) and ICB ( $P0''$ ) to the **a1** acceptor level with participation of TO phonons. However, as it follows from Figure 19 and Table 6, the energy positions of  $P0$ -bands in the case of intercalates  $\text{GaSe}[\text{H}_2\text{O}]$  and  $\text{GaSe}[\text{C}_7\text{H}_8]$  are shifted into the high-energy range.

The intercalation of GaSe crystals with alcohol (Figures 19c and 19f) results in practically total degradation of emission lines related with free excitons and those localized near stacking faults in crystal layers, as well as excitons bound at point defects. In this case, at  $T = 4.5$  K, PL spectra demonstrate only wide weakly structured bands with the peaks at  $606.0 \pm 0.5$  nm ( $P0'$ ,  $P0''$ ) and shoulder close to 614 nm. However, in this case, the integrated intensity of PL spectrum remains practically the same as those in GaSe crystals intercalated with water or toluene. The above energy positions of these bands allow their identification with radiative recombination of carriers from DCB and ICB onto the **a1** acceptor level located near 63 meV above the VB top, which takes place with participation of TO phonons.

According to the data of Table 5, one can show that the energy position of **a1** acceptor level (which for nondoped GaSe crystal is located at 70 meV above the VB top) slows down in the intercalates  $\text{GaSe}[\text{C}_7\text{H}_8]$ ,  $\text{GaSe}[\text{C}_2\text{H}_5\text{OH}]$  and  $\text{GaSe}[\text{H}_2\text{O}]$  by 2.7, 6.7, and 15.8 meV, respectively.

## 5.2. InSe crystals

Shown in Figures 20a to 20f are low-temperature ( $T = 4.5$  K) PL spectra of InSe crystals intercalated with toluene, water, and alcohol for 35 and 165 days. For comparison, shown in Figures 20g and 20h are PL spectra of InSe crystals nondoped and doped with Cd at the concentration 0.01 mass % previously investigated in [19]. The PL spectrum of nondoped InSe crystal (Figure 20g) is superposition of emission lines that correspond to (i) free excitons ( $A$ -line,  $\lambda = 928.0$  nm), (ii) excitons located near stacking faults in crystal layers ( $A_d$  lines), (iii) excitons localized in the density-of-state tails ( $A_t$  lines), and (iv) excitons related with point defects of crystalline structure ( $B1$ – $B6$  lines), which are related with defects by Frenkel and Schottky (see [19]).

Contrary to  $\epsilon$ -GaSe, InSe crystals have rhombohedral symmetry of the crystalline lattice ( $\gamma$ -modification), which is lower than that of  $\epsilon$ -GaSe [2]. Therefore, the partial disordering of crystal layers in InSe results in appearance of stacking faults in layers, namely, the areas of mixed  $\epsilon$ - and  $\gamma$ - modifications. In these areas, the band gap is larger than in the areas of pure  $\gamma$ -modification, and excitons located in the mixed areas possess higher emission energies. The energy positions of the respective lines and  $P0$ -bands at  $T = 4.5$  K are summarized in Table 6.

The intercalation of InSe crystals with molecules of toluene, water, and alcohol, as well as the intercalation time, has an essential influence on their optical properties. It is clearly pronounced (Figures 20a to 20f) in an essential decrease in the emission line intensity of bound excitons ( $B1$ – $B6$  lines) and in the respective growth of emission lines related with free excitons as well as excitons bound with stacking faults in layers and in the density-of-state tails. For comparison, it should be noted that the same changes take place (Figure 20h) in PL spectra of InSe crystals doped with Cd [19] or electrochemically intercalated with hydrogen (see insert in

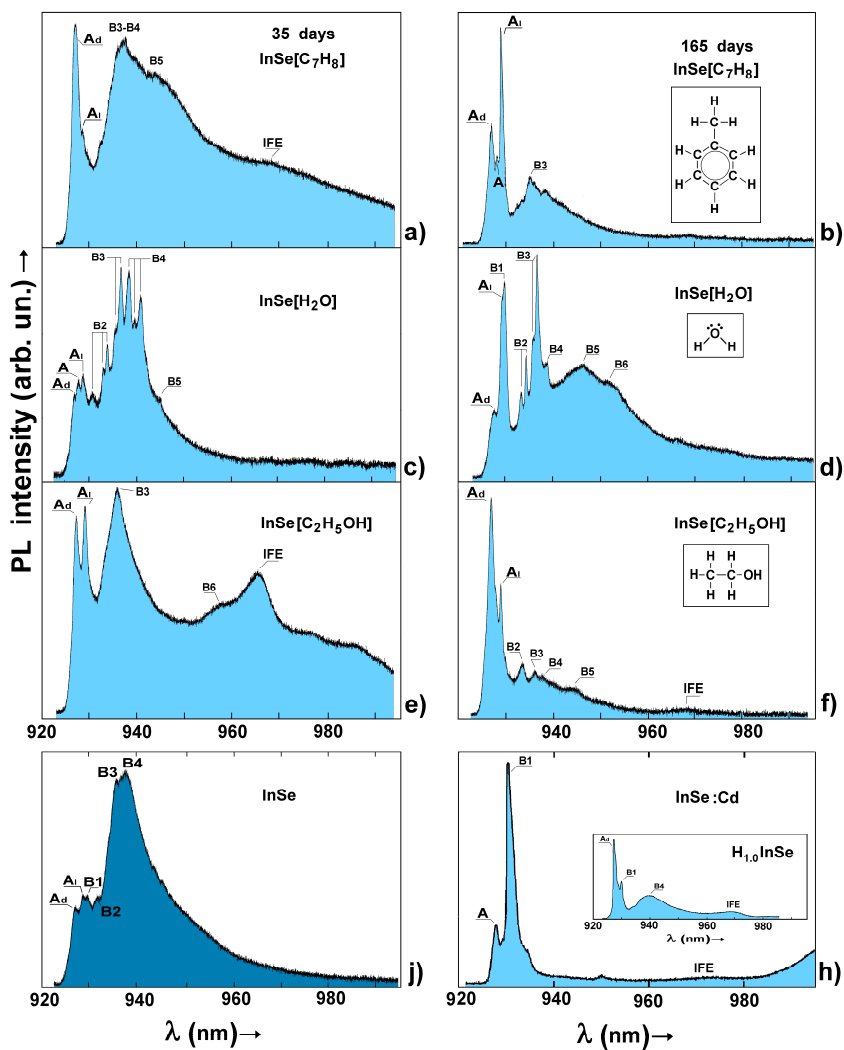


Figure 20. PL spectra of the crystals at the temperature  $T = 4.5$  K: a, b—InSe[C<sub>7</sub>H<sub>8</sub>]; c, d—InSe[H<sub>2</sub>O]; e, f—InSe[C<sub>2</sub>H<sub>5</sub>OH], intercalated for 35 and 165 days, respectively; g—InSe; and h—InSe:Cd [19]. Insert in h—H<sub>1.0</sub>InSe.

Figure 20h). Thereof, contrary to GaSe crystals, intercalation with hydrogen or hydrogen-containing molecules, like to doping with elements of the second group of periodic table, results in essential improvement of the crystalline lattice in InSe crystals.

An increase in the time of intercalating the InSe crystals with toluene, water, or alcohol leads to improvement of PL spectra: A<sub>d</sub> lines begin to dominate, and the emission line of free exciton typical for  $\gamma$ -modification appears in crystals intercalated with toluene. The value of blue shift

observed for  $A_d$  lines in the intercalated crystals relatively to A-line in nonintercalated  $\gamma$ -InSe reaches the value 1.5 meV. It is also typical that B2–B4 lines corresponding to emission of bound excitons in the crystals intercalated with water are split. In this case, the split states are located in the long-wave range relatively standard positions of these lines, and the value of maximum splitting for these lines approaches to 2.0 meV. It is indicative of a rather complex structure of defects that provide bonding these excitons.

Crystal	Wave length of emission line and band peaks (nm)									
	$A_d$	A	$A_1$	B1	B2	B3	B4	B5	B6	IFE
InSe	927.5		929.0	930.0	932.0	936.0	938.0	-	-	-
InSe[C <sub>7</sub> H <sub>8</sub> ] – 35 days	927.0		928.5							968.0
InSe[C <sub>7</sub> H <sub>8</sub> ] – 165 days	927.0	928.0	928.9			935.0				
InSe[H <sub>2</sub> O] – 35 days	926.9	927.9	929.1	-	931.9 933.1 933.9	935.6 936.8	938.5 939.7 941.0	945.0	-	-
InSe[H <sub>2</sub> O] – 165 days	927.6		929.4	929.8	933.3 934.3	935.9 936.5	938.7	946.1	951.9	-
InSe[C <sub>2</sub> H <sub>5</sub> OH] – 35 days	927.3		929.1			936.0			957.4	965.3
InSe[C <sub>2</sub> H <sub>5</sub> OH] – 165 days	926.8		928.9		933.5	936.1	937.6	944.2		968.0
InSe:0.01Cd (data [19 ])		927.9	-	930.2	-	935.5	-	-	950.0	972.0

**Table 6.** Positions of PL lines for free and bound excitons at  $T = 4.5$  K in nonintercalated and intercalated InSe crystals

Besides, in crystals InSe intercalated with alcohol for not so long time (35 days), one can observe the wide band peaking at 966 nm that is caused by radiative recombination of free excitons from indirect conduction band with participation of TO phonons. With increasing the time of intercalation, this band decays.

### 5.3. Discussion

The performed investigations of PL spectra of InSe and GaSe crystals intercalated with toluene, water, and alcohol allows stating that intercalation with HCM that contain carboxyl CH and hydroxyl OH groups exert different influence on optical properties of these crystals. In InSe crystals, intercalation with HCM considerably decreases the intensity of emission lines related with bound excitons, which is a direct confirmation of improvement of the crystalline lattice as a consequence of decreasing the amount of defects responsible for exciton bonding.

Vice versa, in GaSe crystals, increasing the time of intercalation with water and toluene results in enhancing the intensity of radiation from bound excitons, while the structure of the line inherent to free excitons is not practically improved. At the same time, the intercalation of GaSe crystals with alcohol leads to full disappearance of emission lines both of free and bound excitons, which is quite opposite to that observed in InSe crystals. In addition, the intercalation of GaSe crystals with HCM results in lowering the energy position of the **a1** acceptor level relatively to the VB top.

We consider that these differences are caused by peculiarities of covalent bonds inside crystal layers of these crystals. Thus, InSe crystals are more ionic than the GaSe ones [20]. It defines the formation of a great number of various defects, which results in appearance of different type conductivity, namely, *n*-type in InSe and *p*-type in GaSe. To expand discussion, let us consider results of the studies [11, 19], where it was shown that doping the crystals InSe and GaSe with low concentration of impurities (0.01 mass % of Cd or Zn) and the following irradiation with  $\gamma$ -quanta results in the growth of integrated intensity of radiative recombination. This growth takes place on the background of considerable lowering the PL intensity of bound excitons relatively to that of free excitons. In this case (see Figure 20), the PL spectrum of the InSe crystal doped with Cd impurity approaches by its shape and structure to the spectrum of InSe intercalated with hydrogen, toluene, or alcohol.

Vice versa (see [11, 19]), doping the crystals InSe and GaSe with Ge or Sn results in a sharp decay of the integrated intensity of radiative recombination. It allows making an assumption that doping with elements of the second and fourth groups of periodic table influences the growth of these crystals in a different manner. Moreover, even at low concentrations (0.01 mass %), impurities of Cd, Zn, Ge, or Sn are nonuniformly distributed in these crystals, and their concentration can differ almost by one order from one point to another.

At the same time (see [19]), when doping the InSe crystals with Cd or Zn, the type of crystal conductivity changes from *n*- to *p*-type, and in the spectral range after 1.0 mkm (Figure 20h), one can observe the P1–P3 emission bands related with carrier transitions from DCB and ICB to the deep acceptor level as well as transitions between donor and acceptor levels with participation of optical TO phonons. The similar wide bands are also observed in GaSe crystals of *p*-type conductivity after their doping with low concentrations of Cd or Zn impurities [11, 19].

However, contrary to doping the InSe crystals with Cd or Zn, their intercalation with hydrogen or HCM leads neither to changing their type of conductivity nor to appearance of new additional wide bands in the range after 1.0 mkm.

Also in [1], the authors considered the case of passivating the defects with hydrogen atoms in InSe and GaSe crystals of *n*- and *p*-type. According to this work, under electrochemical intercalation of InSe and GaSe crystals with hydrogen, the latter is embedded into interlayer and intralayer spaces and recombines there up to the molecular state. At the same time, a small part of hydrogen remains in the atomic state and passivates point defects in the crystal. When passivating the donor (see Figures 21a and 21b), proton is localized closer to the defect, while passivating the acceptor, proton is more movable. It is confirmed by the fact that in EPR spectra

g-factor and the spectral width in  $H_xInSe$  intercalates are considerably lower than in  $H_xGaSe$  ones [1].

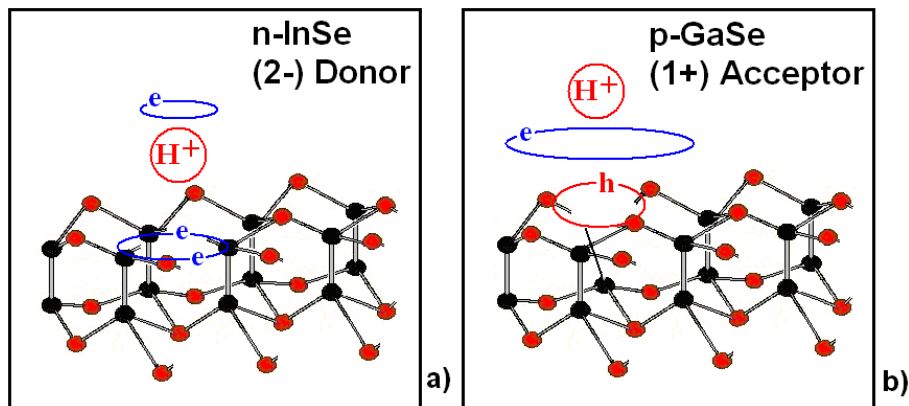


Figure 21. a, b – the simplest defects of donor and acceptor type in  $n$ -InSe and  $p$ -GaSe crystals and the scheme of their passivation with hydrogen.

In accord with [21], passivation with atomic hydrogen also results in lowering the activation energy of donor and acceptor levels, since in  $H_xInSe$  intercalates at low temperatures ( $T = 70$  K) one can observe the growth by one order in the free electron concentration, and the further growth of temperature results in exhaustion of the shallow donor level. The additional optical investigations performed by us also show (see the insert to Figure 20h) that intercalation with hydrogen improves PL spectra of  $n$ -InSe crystals and does not influence on PL spectra of  $p$ -GaSe crystals.

At the same time, when intercalating the crystals with hydrogen, the lattice parameter and width of the van der Waals gap grow due to embedding the hydrogen molecules into interlayer and intralayer spaces [1]. The authors of the work [22] investigating the influence of hydrostatic pressure on lattice parameters in InSe crystals showed that increasing the pressure from  $10^5$  up to  $8 \times 10^9$  Pa results in essential narrowing the van der Waals gap as a consequence of decreasing the distance  $C_{Se-Se}$  between the two nearest Se atoms located in the adjacent layers from 0.38 down to 0.33 nm (13%). Inside crystal layers, the distance  $C_{In-In}$  between neighboring In atoms is decreased from 0.279 down to 0.269 nm (3.58%), and the distance  $C_{In-Se}$  between In and Se atoms—from 2.65 down to 2.59 nm (2.26%). However, as a consequence of the fact that the angle  $\varphi$  between atoms Se–In–In grows from  $119.3^\circ$  up to  $121.3^\circ$  (1.5%), the thickness of crystal layer decreases only by 0.26%—from 0.536 down to 0.5345 nm.

The extrapolation of data from the studies [1, 22] as well as comparison of lattice parameters of InSe [6, 22] and GaSe [5] with sizes of molecules allows to conclude that the natural intercalation of these crystals with molecules of water, alcohol, and toluene results in their embedding into the interlayer space, which causes growth of the van der Waals gap in respective places. In this case, electrochemical intercalation leads to physical sorption of

hydrogen in crystals (since hydrogen can be deintercalated from InSe and GaSe crystals under usual evacuation at the temperatures 110–120°C with participation of full-symmetric half-layer A-phonons able to change the thickness of crystal layers and the intralayer space [1]), while in the case of natural intercalation with water, alcohol, and toluene there takes place chemical sorption of molecules in the interlayer space.

To check up general properties and differences that occur in InSe and GaSe crystals after doping with Cd, Zn, Ge, or Sn atoms, or after intercalation with water, alcohol, and toluene, let us consider the simplest defects typical for these crystals (Figure 21).

In accord with Figure 21a, the absence of Se atom inside the layer makes it impossible to allocate 2/3 portion of electron charge to each of the nearest atoms for the creation of the natural  $sp^3$ -hybrid bond. It is the way with which the simplest (2-) donor arises in *n*-InSe crystals. Simultaneously, the absence of Ga atom in *p*-GaSe crystal (Figure 21b) results in the creation of the (1+) acceptor state since unpaired *s*-electron from the nearest Ga atom provides the hybrid bond with three Se atoms of the upper monolayer.

In the course of doping the *p*-GaSe crystals with impurities Cd or Zn (Figure 21b), it becomes possible for Ga vacancies to be substituted with Cd or Zn atoms with the simultaneous creation of a new (1+) acceptor as a consequence of deficit of one valence electron in Cd or Zn atom. Then there arises a set of absorption and emission bands in the long-wave spectral range, which is caused by transitions of carriers from direct and indirect conduction bands on the deep acceptor level, or by transitions between donor and acceptor levels in *p*-GaSe:(Cd, Zn) crystals.

Doping the InSe crystals with impurities, Cd or Zn changes their type of conductivity. It becomes possible (see Figure 21a) when three upper In atoms are simultaneously substituted with Cd or Zn atoms. This more complex defect becomes the (1+) acceptor. The concentration of impurities near these defects should be higher since it changes the type of conductivity in InSe crystals, which by analogy with the *p*-GaSe:(Cd, Zn) crystals results in appearance of wide bands in PL spectra of *p*-InSe:(Cd, Zn) that are caused by radiative recombination of carriers from DCB and ICB onto the deep acceptor level. Moreover, the availability of another type defects enables to explain the reason for nonuniform distribution of impurities in these crystals.

In the case of crystals intercalated with HCM, embedded molecules, except hydrogen, contain either carbon atoms (toluene, alcohol) or hydroxyl group (alcohol, water). The investigations performed by us showed that the intercalation of *p*-GaSe and *n*-InSe crystals with toluene leads to changes in PL spectra, which are similar to those observed after intercalation with hydrogen. It allows concluding that passivation of defects with toluene is identical to that with hydrogen. However, in the case of toluene molecules, hydrogen ions are symmetrically located relatively to the main axis of the molecule and possess other electro-negativity than those in the methyl tail. It leads to different positions of toluene molecules in the van der Waals gap of *n*-InSe and *p*-GaSe crystals that contain different defects.

Thus, in *n*-InSe crystals intercalated with toluene and hydrogen one can observe “curing” the defects since emission lines of excitons localized on various defects in crystals disappear. By contrast, in the case of *p*-GaSe growth of the intercalation time “worsens” crystal quality—there appear P0-bands, and the emission intensity of bound excitons increases. It can be

possible, when a toluene molecule is differently oriented relatively to (2-) donor and (1+) acceptor. As the (2-) donor has higher electro-negativity, the toluene molecule approaches to this defect with its massive benzene ring and becomes more stabilized in space. In the case of (1+) acceptor, the molecule approaches to the defect with its tail C-H<sub>3</sub>. In this situation, there can take place deviation of the toluene molecule near this defect, which results in decay and binding the excitons as well as to enhancing radiative recombination via the defect centers of this crystal.

Unlike to toluene molecules, those of water and alcohol contain the hydroxyl group OH. In *p*-GaSe crystals, it results in essential growth of the P0-band in PL spectra that is caused by radiative recombination of carriers from DCB and ICB onto the acceptor level a1 with emission of TO phonons. Besides, the intensity of exciton emission is considerably lowered, since water and alcohol molecules, being near the (+1) acceptor, essentially disturb the lattice of *p*-GaSe crystal.

Contrary to *p*-GaSe crystals, in *n*-InSe crystals intercalated with water and alcohol (like those with embedded hydrogen and toluene) curing the point defects takes place. However, in this case (2-) donor is passivated with the hydroxyl group. As the water molecule is more symmetric than the alcohol one, and its size practically coincides with that of defect, it can vary between several symmetric positions relatively to this defect. In the crystal lattice, it results in splitting the exciton state related with this defect.

#### 5.4. Conclusions

The performed investigations of low-temperature ( $T = 4.5$  K) PL spectra of GaSe and InSe crystals intercalated with hydrogen-containing molecules (HCM) of water and alcohol, their comparison with the spectra of GaSe and InSe crystals intercalated with hydrogen or doped with impurities Cd, Zn, Ge, Sn [11, 19], as well as review of the simplest defects carried out in discussion for the crystals of *n*- and *p*-type enabled to explain differences of optical properties inherent to *p*-GaSe and *n*-InSe crystals and to draw the following conclusions:

- i. HCM are predominantly located in the interlayer space and passivate point defects of *p*-GaSe and *n*-InSe crystals.
- ii. The availability of two conductivity types, namely, *p*-type in GaSe and *n*-type in InSe, leads to different influence on their optical properties.

In particular, in *p*-GaSe crystals intercalation with HCM possessing the OH group results in considerable disturbance of the crystalline lattice around the (+1) acceptor, as a consequence of which emission lines inherent to free and bound excitons disappear, while radiative recombination of carriers from DCB and ICB onto the a1 acceptor level located at 70 meV above the VB top grows. This effect of increasing the intensity of radiative recombination of carriers from DCB and ICB onto the a1 acceptor level in *p*-GaSe is observed with increasing the intercalation time as well as when transferring along the direction toluene → water → alcohol.

When transferring from nonintercalated GaSe to the HCM-intercalated ones along the set GaSe → GaSe[C<sub>7</sub>H<sub>8</sub>] → GaSe[C<sub>2</sub>H<sub>5</sub>OH] → GaSe[H<sub>2</sub>O], the energy position of the a1 acceptor level in

the forbidden gap is lowered in accord with the sequence  $70 \rightarrow 67 \rightarrow 63 \rightarrow 56$  meV. By analogy with the *p*-GaSe and *n*-InSe crystals intercalated with hydrogen, it has been made an assumption that the observed lowering the position of activation energy for the a1 acceptor level is caused by passivation of this defect with HCM.

By contrast, in *n*-InSe crystals intercalated with HCM, one can observe curing the point defects, predominantly (2-) donors, which results in the growing intensity of emission lines related with free excitons and practically full disappearance of lines inherent to bound excitons as well as emission bands of indirect free excitons with participation of optical phonons. In this case, the effects of curing the defects in *n*-InSe are more clearly pronounced after intercalation with HCM containing the molecules of carboxyl group (CH) or molecular hydrogen than in those with the hydroxyl group (OH)-water or alcohol.

Also, after the intercalation of *n*-InSe crystals with water, splitting the emission lines of bound excitons is observed, which is caused by splitting the exciton states related with the (2-) donors. However, intercalation with HCM does not practically change the integrated intensity of radiative recombination for excitons and free carriers in *p*-GaSe and *n*-InSe crystals.

## 6. Summary

In this review, in the wide energy range from energies of electron transitions between inner shells of intercalated atoms and those typical for energies of electrons providing valence bonds in the crystalline matrix down to the energies of intrinsic vibrations of atoms (nuclei) of molecules intercalated into the matrix, we have presented the results of investigations by using electron-microscopic, energy-dispersive, and optical methods. These methods allow to study spectra within the range of fundamental electron transitions in the matrix as well as in the range of IR vibrations of intercalated molecules in layered InSe and GaSe crystals with embedded molecular hydrogen or hydrogen-containing molecules (HCM) of water, alcohol, and toluene. Described also have been the methods for the intercalation and deintercalation of HCM.

It has been shown that these crystals in the course of intercalation free take (and during deintercalation release) not only atomic hydrogen but also HCM. This process takes a look of a hysteresis loop—it is retarded during intercalation and is faster during deintercalation when heating and evacuating in a vacuum chamber. Adduced have been the empirical equations relating these two processes and their temporal estimates. We have also determined the optimal dimensions of the crystals (including their powders) to accelerate the process of intercalation-deintercalation.

As InSe and GaSe crystals are characterized by two different types of conductivity, it results, when intercalating with hydrogen and HCM, in predominant recombination of free and bound excitons in *n*-InSe crystals, while in *p*-GaSe crystals processes of free carrier recombination via impurity levels are predominant. These processes have no effect on the integrated intensity of emission from the crystal within the range of fundamental transitions, since the energy of valence electron transitions for HCM lies in the UV range.

The results obtained in this work with account of the conclusions made by us in [1] are indicative of promising applications of these layered matrixes (and powders from them) when creating operation elements of solid hydrogen accumulators. At the same time, these layered InSe and GaSe crystals themselves with different types of conductivity and their thin-layer intercalates as well as other similar compounds can be considered as promising candidates for the creation of various hybrid layered structures for flat flexible displays. The obtained in this work results for various cases of volume dimensions, conditions and terms of their operation can be used for solving these tasks, too.

## Acknowledgements

Performing these investigations became possible owing to the project no. 0108U000252 within the framework of the departmental subject area in the National Academy of Sciences of Ukraine in accord with the Program for Scientific Instrument Engineering.

## Author details

Yuriy Zhirko<sup>\*</sup>, Vasiliy Grekhov<sup>1</sup>, Nikolay Skubenko<sup>1</sup>, Zakhar Kovalyuk<sup>2</sup> and Taras Feshak<sup>2</sup>

<sup>\*</sup>Address all correspondence to: zhirko@nas.gov.ua

1 Institute of Physics National Academy of Sciences of Ukraine, Kiev,, Ukraine

2 Chernivtsy Department of the Institute for Material Science Problems National Academy of Sciences of Ukraine, Chernivtsy, Ukraine

## References

- [1] Zhirko Y, Trachevsky V, Kovalyuk Z. Some physico-chemical aspects of layered crystal application for solid state hydrogen storage. InSe and GaSe crystals. In: Jianjun Liu editor. Hydrogen storage. InTech, 2012, Chapter 9; p. 211–242. (ISBN) 978-953-51-0731-6
- [2] Belen'kii G, Stopachinskii V. Electronic and vibrational spectra of 3–6 layered semiconductors. *Sov. Phys. Usp.* 1983; 26: 497–517.
- [3] Polian A, Kunc K, Kuhn A. Low-frequency lattice vibrations of  $\delta$ -GaSe compared to  $\epsilon$ - and  $\gamma$ -polytypes. *Solid State Commun.* 1976; 9: 1079–1082.
- [4] Ghosh P.H. Vibrational spectra of layer crystals. *Appl. Spectrosc. Rev.* 1983; 19: 259–323.

- [5] Kuhn A, Chevy A, Chevalier R. Crystal structure and interatomic distance in GaSe. *Phys. Status Solidi B*. 1975; 31: 469–473.
- [6] Goni A, Cantarero A, Schwarz U, Syassen K, Chevy A. Low-temperature exciton absorption in InSe under pressure. *Phys Rev B*. 1992; 45: 4221–4226.
- [7] Martines-Pastor, Segura A, Valdes J. Electrical and photovoltaic properties of indium-tin-oxide/p-InSe/Au solar cells. *J. Appl. Phys.* 1987; 62: 1477–1483.
- [8] Lebedev A, Rud' V, Rud' Y. Photosensitivity of heterostructures porous silicon-layered A<sup>III</sup>B<sup>VI</sup> semiconductors. *Fizika i Tekhnika Poluprovodnikov (in Russian)*. 1998; 32: 353–355.
- [9] Shigetomi S, Ikari T. Electrical and photovoltaic properties of Cu-doped *p*-GaSe/*n*-InSe heterojunction. *J. Appl. Phys.* 2000; 88: 1520–1524.
- [10] Grigorchak I, Zasloukin A, Kovalyuk Z, et al. Patent of Ukraine, 2002, Bulletin No. 5, No46137.
- [11] Zhirko Y, Skubenko N, Dubinko V, et al. Influence of impurity doping and  $\gamma$ -irradiation on the optical properties of layered GaSe crystals. *J. Mater. Sci. Eng. B*. 2012; 2: 91–102.
- [12] Kozmik I, Kovalyuk Z, Grigorchak I, Bakchmatyuk B. Preparation and properties of hydrogen intercalated gallium and indium monoselenides. *Izvestija AN SSSR Inorganic materials (in Russian)*. 1987; 23: 754–757.
- [13] Zhirko Y, Kovalyuk Z, Pyrlja M, Boledzyuk V. Application of layered InSe and GaSe crystals and powders for solid state hydrogen storage. In: Vezirogly N et al editors. *Hydrogen Materials Science and Chemistry of Carbon Nano-materials*. Springer ©; 2007 p.325–340.
- [14] Zhirko Y, Kovalyuk Z, Klad'ko V. et al. Investigation of hydrogen intercalation in layered crystals InSe and GaSe. In: *Proceedings of (HTM-2007) 15 International Conference Hydrogen Economy and Hydrogen Treatment of Materials*; 21–25 May 2007; Donetsk, Ukraine. 2007. 2, p. 606–610.
- [15] Zhirko Y, Kovalyuk Z, Pyrlja M, Boledzyuk V. Optical investigation of hydrogen intercalation–deintercalation processes in layered semiconductor  $\gamma$ -InSe crystals. In: *Hydrogen Materials Science and Chemistry of Carbon Nanomaterials*. NATO Science Series II: Mathematics, Physics and Chemistry. 2004; 172. p. 519–530.
- [16] Demchina L, Kovalyuk Z, Mintjanskii I. Ohmic contacts preparation for A3B6 layered crystals. *Pribery I Tekhnika Eksperimenta*. 1980; 2: 219–221.
- [17] Grigorchak I, Kovalyuk Z, Yurtzenjuk S. Preparation and properties of intercalated A<sup>III</sup>B<sup>VI</sup> layered junctions. *Izvestija AN SSSR. Ser. Neorg. Mater.* 1981; 17: 412–415.

- [18] Zhirko Y. Role of intrinsic defects in the process of synthesizing the layered crystals GaSe. In: Proceedings of 14-th European Conference of Solid State Chemistry (ECSSC14). 7–10 July 2013; Bordeaux. France. p.139
- [19] Zhirko Y, Skubenko N, Dubinko V, Kovalyuk Z, Sydor O. Influence of  $\gamma$ -Irradiation on the Optical Properties of Pure or Impure Zn, Cd and Ge-Doped Layered InSe Crystals. *J. Mater. Sci. Eng. B.* 2013; 3:162–174.
- [20] Nakanishi F, Matsubara T. Note on ionisity of kayered conhouds GaS, GaSe, and InSe. *J. Phys. Soc. Japan.* 1982; 516: 1339–1340.
- [21] Zhirko Y, Kovalyuk Z, Zaslonkin A, Boledzyuk V. Photo and electric properties of hydrogen intercalated InSe and GaSe layered Crystals. In: Proceedings of Int. Confer. Nano/Moleclar Photochemistry and Nanomaterials for Green Energy Development (Solar'10). 15–17 February 2010; Cairo, Egypt; 2010. p. 48–49.
- [22] Olguin D, Cantarero A, Ulrich C, Suassen K. Effect of pressure on structural properties and energy band gaps of  $\gamma$ -InSe. *Phys. Status Solidi B.* 2003; 235: 456–463.